catalysts

MDPI

Review

The Influence of Synthesis Methods and Experimental Conditions on the Photocatalytic Properties of SnO_2: A Review

Jéssica Luisa Alves do Nascimento [1], Lais Chantelle [2], Iêda Maria Garcia dos Santos [2], André Luiz Menezes de Oliveira [2,*] and Mary Cristina Ferreira Alves [1,*]

[1] Laboratório de Síntese Inorgânica e Quimiometria (LABSIQ), Departamento de Química, CCT, Universidade Estadual da Paraíba, Campus I, Campina Grande 58429-500, PB, Brazil; jessica_alvesn@yahoo.com

[2] Núcleo de Pesquisa e Extensão: Laboratório de Combustíveis e Materiais (NPE/LACOM), Departamento de Química, Universidade Federal da Paraíba, Campus I, João Pessoa 58051-900, PB, Brazil; lais.chantele@hotmail.com (L.C.); ieda@quimica.ufpb.br (I.M.G.d.S.)

* Correspondence: andrel_ltm@hotmail.com (A.L.M.d.O.); mary.alves@cct.uepb.edu.br (M.C.F.A.)

Abstract: Semiconductors based on transition metal oxides represent an important class of materials used in emerging technologies. For this, the performance of these materials strongly depends on the size and morphology of particles, surface charge characteristics, and the presence of bulk and surface defects that are influenced by the synthesis method and the experimental conditions the materials are prepared. In this context, the present review aims to report the importance of choosing the synthesis methods and experimental conditions to modify structural, morphological, and electronic characteristics of semiconductors, more specifically, tin oxide (SnO_2), since these parameters may be a determinant for better performance in various applications, including photocatalysis. SnO_2 is an n-type semiconductor with a band gap between 3.6 and 4.0 eV, whose intrinsic characteristics are responsible for its electrical conductivity, good optical characteristics, high thermal stability, and other qualities. Such characteristics have provided excellent results in advanced oxidative processes, i.e., heterogeneous photocatalysis applications. This process involves semiconductors in the production of hydroxyl radicals via activation by light absorption, and it is considered as an emerging and promising technology for domestic-industrial wastewater treatment. In our review article, we focused on the photodegradation of different organic dyes and types of persistent organic pollutants using SnO_2-based photocatalysts, and how the efficiency of these materials can be impacted by synthesis methods and experimental conditions employed to prepare them.

Keywords: synthesis method; experimental conditions; tin oxide; heterogeneous photocatalysis; persistent organic pollutants; dyes

Citation: do Nascimento, J.L.A.; Chantelle, L.; dos Santos, I.M.G.; Menezes de Oliveira, A.L.; Alves, M.C.F. The Influence of Synthesis Methods and Experimental Conditions on the Photocatalytic Properties of SnO_2: A Review. *Catalysts* **2022**, *12*, 428. https://doi.org/10.3390/catal12040428

Academic Editors: Gassan Hodaifa, Antonio Zuorro, Joaquín R. Dominguez, Juan García Rodríguez, José A. Peres and Zacharias Frontistis

Received: 18 February 2022
Accepted: 4 April 2022
Published: 11 April 2022

1. Introduction

For decades, the world has been affected by serious environmental problems, especially water resources that have been polluted over the years. In particular, the disposal of domestic-industrial effluents in water bodies has been a major problem for modern society [1–5]. In this sense, the research community, public agencies, and environmentalists have been very concerned about this issue. Among the contaminants commonly present in wasters, persistent organic pollutants (POPs) are considered one of the main substances. POPs are heterogeneous synthetic compounds based on carbon from natural or from anthropogenic origins, with a high chemical resistance to degradation in the environment. These substances are characterized by a high level of toxicity and can be disruptive, neurotoxic, or immunosuppressive [6–9]. The excessive presence and accumulation of POPs in food chains has a major impact on human health and well-being. For instance, Mansouri and Reggabi [10] reported that the exposure to endocrine disruptors, and especially POPs, may contribute to the development of type 2 diabetes mellitus. According to these authors,

diabetic subjects had higher plasma concentrations of POPs than non-diabetics, and environmental exposure to some POPs is associated with an increased risk of type 2 diabetes in the studied samples. In addition, authors have stated that the exposure to some other POPs may increase health problem risks [11,12].

The elimination, restriction, and control of POPs took place first in 2001, after the Stockholm Convention [13]. Currently, more than 35 (thirty-five) POPs are reported in literature, such as polychlorinated biphenyls (PCBs), dichlorodiphenyltrichloroethane (DDTs), and hexachlorocyclohexane isomers (HCHs), which are general types of drugs and medicine, pesticides, and synthetic dyes [14–17]. In this context, the search for new methodologies to promote full POP removal and degradation from the environment has attracted too much attention of the scientific community as well as public agencies, but it has also been a challenge to be faced today [18]. Different physical, chemical, and biological methods are used for degrading and removing pollutants present in water, air, and soil, among which adsorption [19,20], electrocoagulation [20], and advanced oxidative processes (AOPs) [21,22].

Among the diversity of water treatment methods, AOPs, particularly, represent a group of techniques characterized by the generation of highly oxidizing agents as free radicals. AOPs stand out due to their high efficiency in the degradation of numerous organic compounds, such as pesticides, surfactants, chlorophenols, and benzene, among others. APOs can promote mineralization of pollutants by transforming them into carbon dioxide, water, and inorganic anions [23–25]. AOPs are divided into homogeneous and heterogeneous, as well as photochemical and non-photochemical, processes [26]. Particularly, the heterogeneous photochemical process known as heterogeneous photocatalysis is one of the most important AOPs techniques used nowadays for being considered a promising technique for the treatment of domestic-industrial effluents and environmental decontamination [23,24,27–29]. In this process, semiconductors are irradiated by a light source (UV and visible light or even sunlight) with energy greater than or equal to its bang gap energy (*Eg*)—the minimum energy required to excite electrons from the lower energy band (valence band, VB) to a higher energy band (conduction band, CB) of a semiconductor. Thus, the energy absorption results in electronic excitation from VB to the CB, which leads to the formation of photoinduced charge pairs (e^-/h^+). Electron–hole pairs present very positive electrochemical potentials, which, when generated, give the semiconductor its redox properties [27,30].

During photocatalysis, photogenerated e^-/h^+ can migrate to the surface of the material and interact with an adsorbed species; in addition, they can be captured in intermediate energy states, or undergo recombination. When e^- are in the BC, one of the very important reactions can occur, which is the reduction of the adsorbed O_2 on the catalyst surface to superoxide ($^{\bullet}O_2^-$) radicals, avoiding recombination of electrons and the hole. This results in the accumulation of an oxygen radical species that can participate in photocatalytic reactions. On the other hand, when h^+ from the the VB migrates to the catalyst surface, it can react with adsorbed H_2O to generate hydroxyl ($^{\bullet}OH$) radicals, reacting with the pollutants to be degraded. It is worth mentioning that electronic recombination does not favor photocatalysis, because if the e^- and h^+ recombine, the formation of the photogenerated e^-/h^+ pairs fails to participate in the oxidation-reduction process and formation of free radicals in the process [30–32]. An illustration of the general mechanism involved in photocatalysis is given in Figure 1, as also reported in [33].

A great variety of semiconductors have been playing an important role in the heterogeneous photocatalysis for energy production from water splitting [34–36] and for environmental remediation toward the degradation of different organic pollutants such as POPs [36–38]. Within the broad range of oxide semiconductors applied in photocatalysis, wide band gap ones, such as SnO_2 [39,40], TiO_2 [41,42], ZnO [43], NiO [44], and WO_3 [45–47], have been extensively explored because they are considered good semiconductors and have showed promising results. Although most studies have been dedicated to titanium oxide (TiO_2), tin oxide (SnO_2) is also worth mentioning, as indicated by

the number of published research articles listed in Table 1. SnO_2 is an n-type semiconductor with a large band gap value between 3.6 and 4.0 eV [47,48]. Its intrinsic characteristics are responsible for the material's conductivity, good optical and electrical characteristics, and high thermal stability, among other qualities. Furthermore, SnO_2 presents a high oxidation potential and chemical inertness, as well as corrosion resistance and non-toxicity [47]. Thus, SnO_2 has been successfully used in heterogeneous photocatalysis and showed to be very efficient in the degradation of different organic pollutants, especially dyes [49–51].

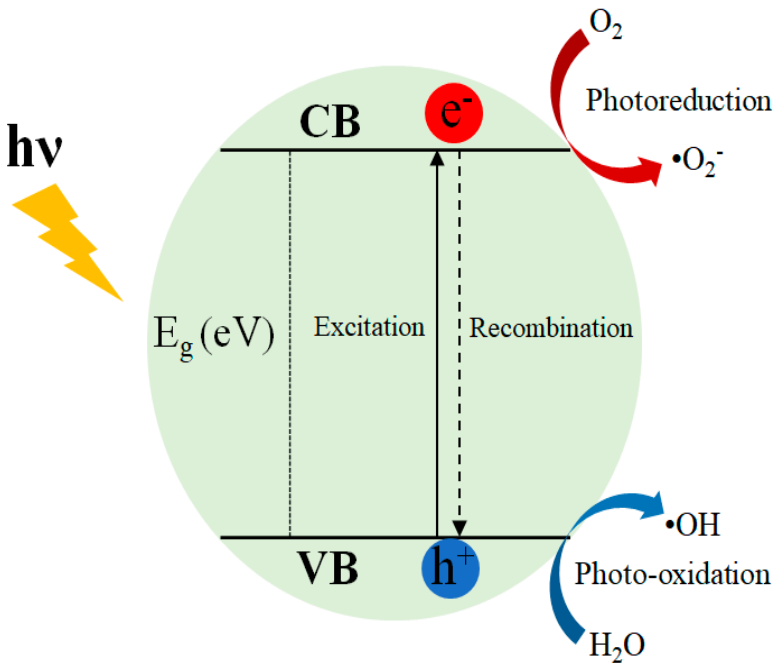

Figure 1. General mechanism of the heterogeneous photocatalysis using a hypothetical semiconductor.

In respect to the synthesis of SnO_2 that can affect the material properties and applications, the photocatalytic ones can be easily modified according to the synthesis route used to prepare the material. In addition, although most SnO_2-based photocatalysts are explored in their powder form, their separation and reuse after the process is difficult, as it needs filtration to recover the catalyst. Thus, other researchers have prepared SnO_2-based catalysts in their film form, which is considered an effective approach to overcome the filtration issues after a photocatalytic reaction, allowing the reusability of the catalyst without any material loss. These factors are important to design new and efficient photocatalysts.

Some review articles have dealt with the applications of SnO_2 materials in photocatalysis. However, to our knowledge, none of them draw attention to particular characteristics of synthesis methods and experimental conditions used to prepare the different SnO_2-based photocatalysts and how these directly impacted the sample characteristics, properties, and photocatalytic efficiency for organic dyes degradation. For instance, in the review published by Al-Hamdi et al. [47], results from studies conducted up to 2017 were shown, which focused on the applications of SnO_2 in an advanced oxidative process for the degradation of organic pollutants, such as phenols, phthalates, and other toxins in water. In addition, authors listed relevant investigations on fundamental aspects related to SnO_2, such as structure and properties, the charge transfer mechanism involved, and parameters that affect the photodegradation of pollutants in aqueous solutions, such as the catalyst load, concentration of the contaminant, and pH. In a recent review, Sun et al. [48] discussed the importance of employing SnO_2-based photocatalysis in environmental science and energy fields. The authors focused several studies dealing with strategies used to enhance the SnO_2 properties for photocatalysis. The effect of doping, formation of solid solutions, stoichiometry, particle size and morphology, besides the formation of hierarchical, porous, and heterojunctions structures, were demonstrated. Apart from the applications in water

splitting and organic dyes photodegradation, the authors discussion gave examples of SnO_2 applications in Cr(VI) and CO_2 reduction. The authors also mentioned the complexities of applying photocatalysts in a large scale to simulate the real scope of the industry since, although significant progress has been achieved in the improvement of the photocatalytic efficiency of SnO_2, there are still major challenges to be faced.

Table 1. Metal oxides applied in heterogeneous photocatalysis of dyes over the last 5 years. Data collected from different research literature databases on 20 January 2022.

Oxide	Publications Attributed to Photocatalysis of POPs	Database	Publications Attributed to Photocatalysis of Dyes	Database
TiO_2	9.103	Scopus	2.132	Scopus
	1.369	Web of Science	3155	Web of Science
	2.492	ScienceDirect	3.933	ScienceDirect
	1.364	ACS Journal Search	1679	ACS Journal Search
ZnO	2.862	Scopus	1251	Scopus
	252	Web of Science	1759	Web of Science
	4.558	ScienceDirect	7.659	ScienceDirect
	542	ACS Journal Search	806	ACS Journal Search
NiO	346	Scopus	93	Scopus
	27	Web of Science	138	Web of Science
	1.164	ScienceDirect	1.500	ScienceDirect
	171	ACS Journal Search	174	ACS Journal Search
SiO_2	582	Scopus	149	Scopus
	41	Web of Science	150	Web of Science
	228	ScienceDirect	343	ScienceDirect
	438	ACS Journal Search	439	ACS Journal Search
WO_3	951	Scopus	135	Scopus
	10	Web of Science	191	Web of Science
	2.593	ScienceDirect	341	ScienceDirect
	2.570	ACS Journal Search	312	ACS Journal Search
SnO_2	425	Scopus	181	Scopus
	21	Web of Science	239	Web of Science
	173	ScienceDirect	330	ScienceDirect
	191	ACS Journal Search	261	ACS Journal Search

Based on what was mentioned, the present work aims to address important aspects about recent and relevant achievements of how the choice of the appropriate synthesis method and experimental parameters may influence the morphology, particle size, bandgap energy, and, consequently, the impact on the photocatalytic properties of SnO_2 for the degradation of different organic dyes as targets of persistent organic pollutants (POPs) molecules. Apart from the applications of pure SnO_2 toward the degradation of dyes, studies concerning photocatalysis using metal and nonmental-doped SnO_2, as well as SnO_2-based composites, are also summarized. We believe that this literature review may provide important aspects for the better development of SnO_2-based catalysts, and understanding the limitations, in order to use them in practical devices.

2. Persistent Organic Pollutants (POPs), Dyes, and Photocatalysts

Environmental problems, and especially water resources, have been a major problem for the population, researchers, and environmentalists [1,2]. There are several contaminants that are usually disposed into the environment, and can be classified into different types, depending on their purpose and origin: persistent organic pollutants (POPs), pharmaceuticals and personal care products (PPCPs), endocrine disrupting chemicals (EDCs), and agricultural chemicals (pesticides, herbicides) [51–53]. Particularly, persistent organic pollutants (POPs)—which are organic chemicals that are highly toxic to humans—animals,

and vegetation stand out among these pollutants. The specific effects of POPs can include allergies, cancer, and damage to the central and peripheral nervous system and reproductive, endocrine, and immune systems [13,14,54].

According to the Stockholm Global Conference held in 2001 that aimed to discuss the consequences of the environmental degradation, twelve (12) chemical substances were included into the POPs class. However, thirty-five (35) POP substances are listed as most harmful [13,15,21,55–59]. Amongst the variety of POPs, drugs, pesticides, hormones, dyes, synthetic textile products, artificial sweeteners, some micro-organisms, and algae toxins have extensively been introduced on a large scale into the environment, which can strongly affect aquatic life and human beings [21,53]. Particularly, synthetic organic dyes stand out for being considerably used over the years in several technological sectors, such as textile industries, in medicine, and in the manufacturing process of pens, among others.

Synthetic dyes are classified as POPs because of their difficulty to be degraded and removed from the environment [55]. The disposal of effluents from textile industries is one of the main sources of pollutants responsible for changes in the quality of receiving water. The different dyes used in textile industries generally have a high organic load, and this can be very harmful to the environment if inappropriately discharged. There is an estimate that about 20% of the dyes used are disposed in effluents because of losses during the dyeing process [36,59,60]. In this context, several methods (chemical, physical, and biological) have been used for dealing with the treatment of contaminated effluents with POPs (Figure 2). However, great efforts have been dedicated to studies related to photodegradation and mineralization of organic dyes using photocatalytic materials under UV-visible light, as well as sunlight irradiation.

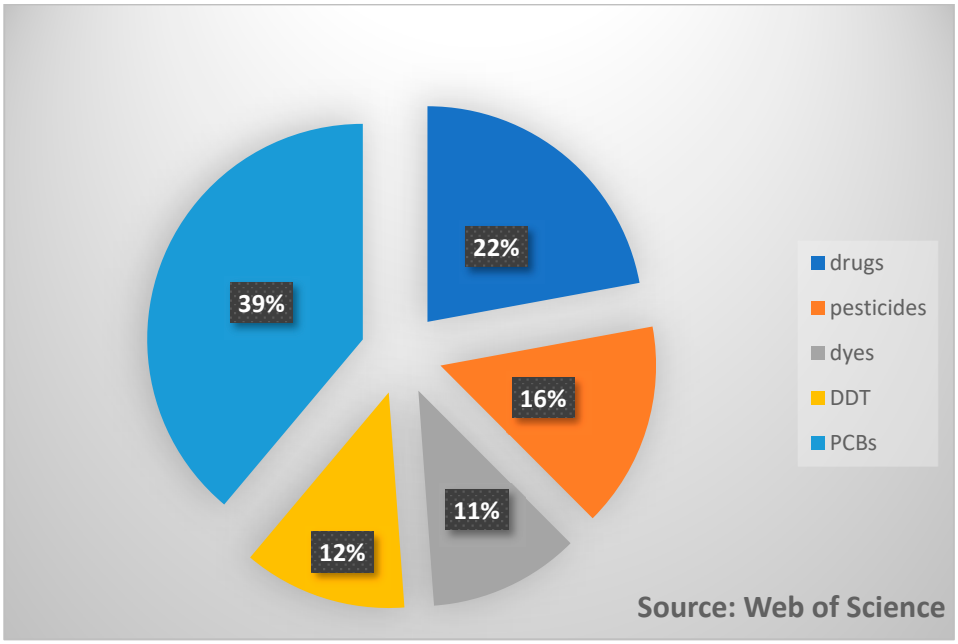

Figure 2. Published articles referring to the treatment of different persistent organic pollutants. Data collected from Web of Science on 20 January 2022.

As aforementioned, different materials have been applied in heterogeneous photocatalysis, especially for photodegradation of POPs. As this review aimed to discuss important works involving the photodegradation of organic dyes and types of POPs, the article's search was done considering different databases, as listed in Table 1. It is important to highlight that most of the publications have devoted to the application of TiO_2-based photocatalysts. However, different metal oxides have been explored for such purposes because of their unique and prominent properties, due to their structure, particle size, and morphology [61]. From this search, SnO_2 appears in 6th place among the six (6) oxide-

based photocatalysts used in photocatalysis of organic dyes. It is still important to mention that scientific research based on tin materials has been increased over the last years.

It is important to highlight that the search was done using the following words for articles dealing with photodegradation of POPS, such as for SnO_2: "SnO_2, photocatalysis and POPs" and "tin oxide, photocatalysis and POPs"; while for works concerning photodegradation of dyes included, "SnO_2, photocatalysis and dyes" and "tin oxide, photocatalysis and dyes". A similar search has been completed for each metal oxide listed in Table 1. Compound words such as "photocatalytic properties", "photocatalytic efficiency", and "organic dyes" were not placed in quotes for the search of papers related to photocatalysis of dyes using these oxides.

Considering organic dyes, additional studies dealing with these pollutants are in need. For instance, the emission of effluents from textile industries is one of the main things re-sponsible for alterations in water bodies' quality. Organic dyes have a high organic load, generating strong impacts on the environment when inappropriately discharged. Depending on the type of dye and the place where it is discarded, they can react with other substances present in the environment, originating mutagenic and carcinogenic by-products [62,63]. In dye molecules, two important organic groups are present: the chromophore one, which is responsible for the color by light absorption, and the auxochrome group that is responsible for dye fixation on fibers and for color intensification. These groups are constituted by conjugated systems with double bonds and functional groups (auxochromes), which are electron donors or acceptors [64]. Such characteristics have made dyes one of the great villains in the process of polluting water. In this context, a great amount of research has explored the photocatalysis of different organic dyes using wide band gap semiconductors, such as SnO_2. These works are discussed as follows for SnO_2, which has been gaining prominence in this type of application over the years, as shown in Figure 3.

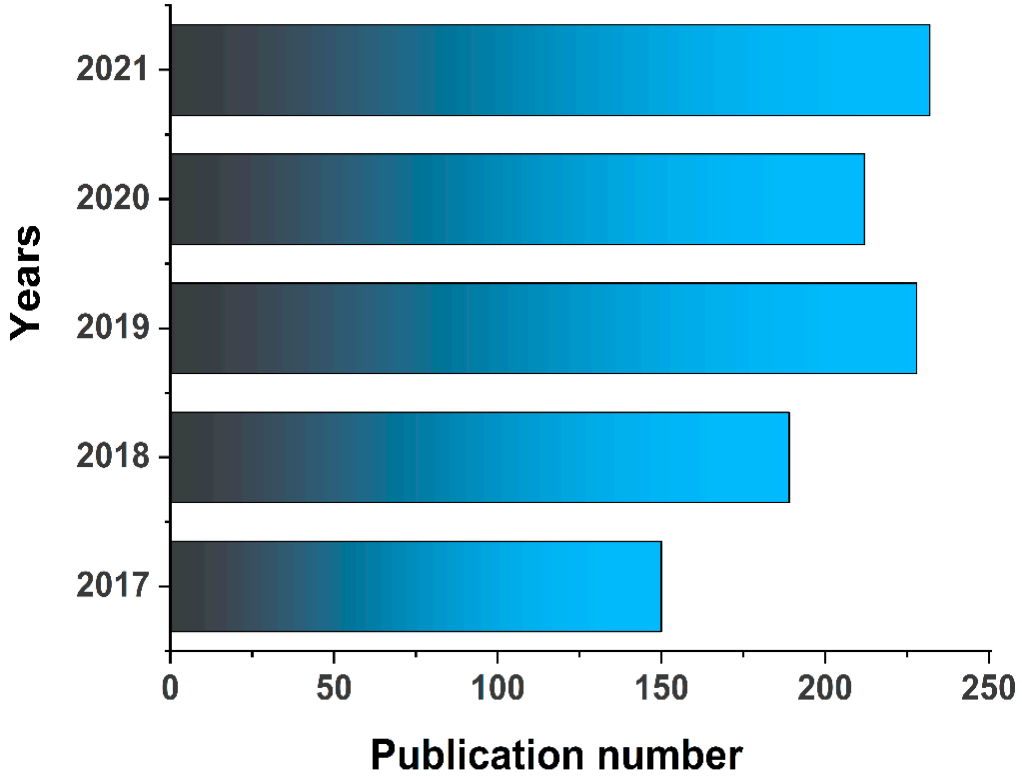

Figure 3. Number of published articles concerning the photodegradation of organic dyes using SnO_2-based photocatalysts. Search performed on 20 January 2022, using different databases. The period of 2017–2021 was considered for this search.

3. Tin-Oxide-Synthesis, Structure, Properties, and Applications as Heterogeneous Photocatalysts

Tin dioxide (SnO_2), obtained by combining Sn^{4+} and O^{2-}, is a ceramic material that has been used in a wide variety of applications, such as gas sensors, photovoltaic energy converters, and photocatalysts [65–67]. The success for multiple applications of SnO_2 is due to its intrinsic characteristics, such as: n-type conductivity, which is responsible for the conductivity of the material, and in addition to optical and electrical characteristics, high thermal stability, and high surface area [36,49,68]. Electrical conductivity can be described in terms of the movement of negatively charged electrons, and this gives rise to an n-type semiconductor [36,49,50,69–71].

As for the crystal structure of SnO_2, at room temperature, it adopts a rutile-type tetragonal structure (cassiterite) with *P42/mnm* space group, as illustrated in Figure 4. This structure is formed by a tetragonal unit cell defined by three (3) parameters: the *a* and *c* lattice parameters and the internal parameter, *u*, which defines the oxygen position (*u*, *u*, and 0). At room temperature, the theoretical lattice parameters for SnO_2 are a = 4.7374 Å, c = 3.1864 Å [72], and u = 0.3056 Å. It has been reported that SnO_2 can also adopt an orthorhombic, $CaCl_2$-type (*Pnnm*) structure, besides existing in an orthorhombic α-PbO_2-type (*Pbcn*), a cubic pyrite-type (*Pa*-3), an orthorhombic ZrO_2-type (*Pbca*), and a cotunnite-type (*Pnma*) structure. However, these structures are metastable at ambient conditions, and it is hard to follow these phase transitions through traditional methods under low pressure and temperatures [63,64].

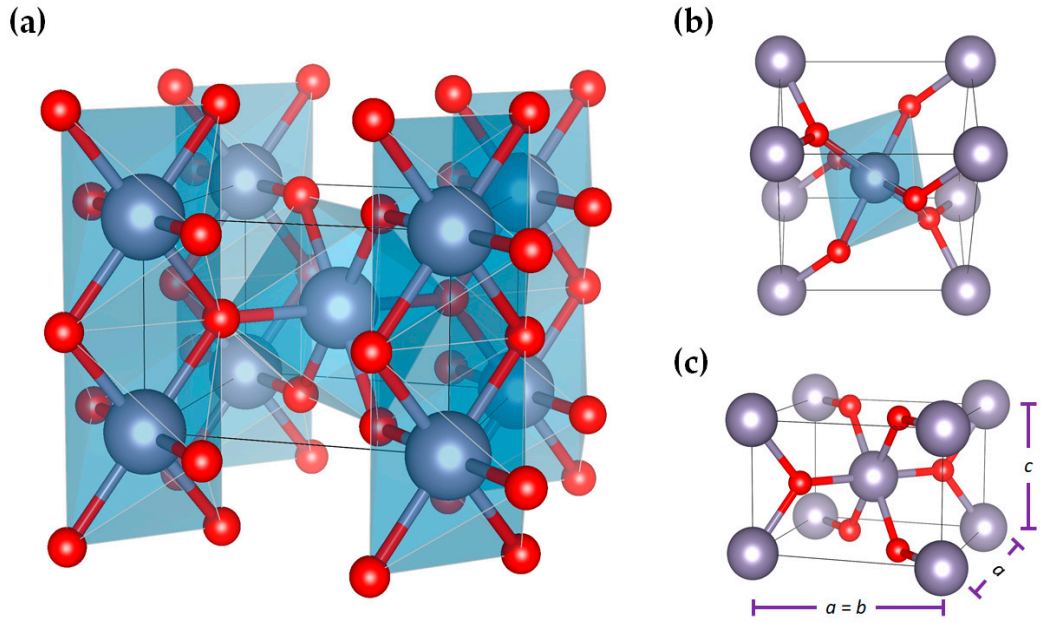

Figure 4. (**a**) A *P42/mnm* tetragonal crystal structure of SnO_2 showing (**b**) environment of distorted SnO_6 octahedron and (**c**) lattice parameters, obtained using VESTA software and structural parameters reported in [73].

The structure of SnO_2 consists of chains of SnO_6 octahedra in which each Sn atom is octahedral, surrounded by six oxygen atoms, while each oxygen is surrounded by three Sn atoms arranged at the corners of an equilateral triangle. The structure's Sn:O coordination is 6:3, with each octahedron not being regular, showing a slight orthorhombic distortion [72,73].

The literature has reported that SnO_2 can present nano- and micro-structured characteristics, however, most researchers have been dedicated to the synthesis of SnO_2 in the form of nanoparticles. Such characteristics have offered good opportunities to explore new physical and chemical applications. Recently, SnO_2 has been applied to the degradation of antibiotics [74], fuel cell catalysts [73], gas sensors [75], sodium ion batteries [76],

light-emitting diodes [77], heterogeneous photocatalysis, and antimicrobial activity [78,79]. There are several synthesis routes and experimental conditions to obtain SnO_2 in powder form, the choice of which may influence the particles' morphology and texture, besides their structural, optical, and electronic properties, which will consequently impact the efficiency and final application of the material. In relation to SnO_2-based thin films, chemical deposition methods have appeared to be the most used [62,80–84].

With respect to the applications in photocatalysis, SnO_2 catalysts with a tetragonal, rutile-type structure are the main phases investigated, but a recent work reported that the coexistence of mixed tetragonal–orthorhombic phases affected the photocatalytic efficiency of SnO_2 [85]. All these factors are described below.

4. Synthesis Methods and the Influence of Experimental Parameters on the Characteristics and Photocatalytic Properties of SnO_2-Based Materials

One of the main aspects this review refers to is the approach of how different synthesis methods and experimental parameters affect the photocatalytic properties of SnO_2-based materials.

Researchers have employed different methods to produce new materials with specific properties and applications. The choice of an appropriate condition to prepare a material is crucial to modifying its physicochemical characteristics, such as crystal structure and morphological and texture characteristics of the particles (size, shape, surface area, and surface charge characteristics), as well as the electronic and optical properties. The variation on these characteristics may change the applicability of the material. In this sense, different researchers have devoted to obtaining SnO_2-based materials with specific characteristics and efficient photocatalytic behaviors. Among the great variety of methods known in the literature, SnO_2-based photocatalysts have been obtained, in their powder form, by a solvothermal reaction [86,87], the microwave-assisted hydrothermal method [88], chemical precipitation [68], the polymeric precursor method [89], and sol-gel [14], all which are mostly used.

In relation to the photocatalytic properties of SnO_2 particles, although there is a variety of organic pollutants, organic dyes such as Methylene blue (MB), Rhodamine B (RhB), and Methyl orange (MO) have been the most used as target molecules to evaluate the photocatalytic efficiency of SnO_2. However, other organic dyes such as Congo red (CR), Malachite green (MG) and Eriochrome black T (EBT) have also been explored for such purposes. In this context, the photodegradation of these organic dyes is highlighted in this review. Apart from powdered SnO_2 materials, SnO_2-based films have also been used as photocatalysts for dye photodegradation [90–93]. For the preparation of films, chemical [64,80,84,86,89] and physical-based deposition methods [64] are used. In the following sections, photocatalytic applications of pure and doped SnO_2-based catalysts, as well as the composites based on SnO_2 in powdered and film forms prepared by different techniques, are also discussed.

4.1. Pure SnO_2-Based Photocatalysts

Besides being synthesized in its pure form, SnO_2 has been prepared in its doped form with metals or nonmetal ions, as well as in the form of composites with other semiconductor materials, or even impregnated in inert, non-active photocatalytic materials. It is well known that the generation of electrons/holes (e^-/h^+) pairs by absorption of a photon of equal energy, to or higher than the band gap energy induced by light, is a basic prerequisite for a semiconductor to be used in photocatalysis. Because of its wide band gap of SnO_2 (3.6 eV), no absorption response to the visible light would be achieved, and this is the main disadvantage of this material, which restricts its application in practical devices. A wide variety of pure semiconductor materials, particularly SnO_2, have been investigated regarding the photocatalytic properties, but only few of them are considered effective photocatalysts.

Besides the value of the forbidden band energy corresponding to absorption in the visible region, it is required that the energy levels of the conduction and valence bands are suited to the redox potential of the water, so as to produce reactive agents to promote breaking of organic pollutants molecules. Therefore, different authors have employed various synthesis methods and varied experimental conditions in order to change particle characteristics, which include size, morphology, and texture, as well as the crystallinity and the presence of defects, in order to design efficient photocatalysts under UV irradiation. These parameters can play an important role during photocatalysis, as they can affect the adsorptive and photo-absorption capacity of the catalyst, besides reducing photogenerated changes of recombination during photoexcitation. In addition, some authors also explored the reaction mechanisms involved in the photodegradation of the dyes and how the reactive species act for the photocatalysis to occur. These points are discussed throughout the review.

For instance, considering pure tin oxide as a photocatalyst, Akram et al. [90] prepared SnO_2 nanoparticles by the continuous microwave flow synthesis (CMFS) method in a domestic microwave oven operating at 600 W, using tin chloride pentahydrate ($SnCl_4 \cdot 5H_2O$), sodium hydroxide (NaOH), ethanolic solutions. The solutions were pumped through the microwave with the aid of peristaltic pumps to attain 10 min of retention time inside the device. The resulting suspension was filtered, washed, and dried at 80 °C for 12 h, followed by heating at 200 °C for 2 h to obtain SnO_2 samples. The photocatalytic properties of the nanoparticles were investigated toward the photodegradation of Methylene blue (MB) dye under UV irradiation (365 nm). In their study, the authors also investigated the effect of the concentration of the reacting $SnCl_4 \cdot 5H_2O$ and NaOH materials on the crystallinity, particle size, and morphology, as well as the photocatalytic behavior of the SnO_2 nanoparticles. The authors evidenced that crystalline SnO_2 samples with tetragonal, rutile-type structures were obtained only after heating at 200 °C. The increase in the concentration of $SnCl_4 \cdot 5H_2O$ (from 0.25 to 0.75 M) and NaOH (from 1 to 3 M) provoked an increase in sample crystallinity and an average particles size from 4.33 to 8.56 nm, with no meaningful change in morphology. This phenomenon was attributed to the increased number of nuclei sites formed by the reacting species, as well as to the microwave irradiation that favors better nucleation and crystal growth. Surprisingly, a decrease of the band gap (*Eg*) values from 3.33 to 3.19 eV was also observed as a function of the precursor's concentration, and it was associated to the increase of the particle size. In relation to the photocatalytic property of the samples, that sample was prepared using the lower concentration of the reacting species, which presented the lowest degree of crystallinity (63%), smallest particle size (4.43 nm), largest surface area (153.57 $m^2\ g^{-1}$), and widest band gap (3.33 eV), and this was the most efficient in the photodegradation of MB dye, reaching up to 93% of degradation in 240 min. According to the authors, the higher efficiency observed for that sample was mainly due to the large surface area and higher concentration of defects.

Still considering pure tin oxide photocatalysts, Abdelkader et al. [92] synthesized SnO_2 nanoparticles via a sol-gel method and calcined it at different temperatures (80, 450, and 650 °C) for 4 h, in order to achieve different crystallinity and particle morphology. The authors investigated the photocatalytic efficiency of the synthesized samples toward Congo red (CR) dye degradation under UVA irradiation. For the synthesis of the nanoparticles, tin chloride ($SnCl_2\ 2H_2O$) was dissolved in 250 mL of deionized water to obtain a white suspension of a 0.4 M Sn (II) concentration. The suspension was stirred for 1h at room temperature and oxalic acid was added dropwise to the aqueous solution as a chelating agent with a molar ration of 1:1 (oxalic acid: tin cations). The obtained suspension was centrifuged, filtered, and washed several times to eliminate chloride ions. The washed precipitate was dried at 80 °C/24 h and calcined at 450 to 650 °C for 4 h. According to the results, the sample obtained after drying at 80° for 24 h (SnO_2-80) crystallizes in pure tin oxalate (SnC_2O_4) with a monoclinic structure. On the other hand, pure SnO_2 with a *P42/mnm* tetragonal, rutile-type structure was obtained after calcinations at 450 (SnO_2-450) and 650 °C (SnO_2-650). The authors draw attention to the use of oxalic acid as a chelating agent, and it affected the particle characteristics for controlling the nucleation and crystal

orientation, as well as the calcination temperature in the control of the crystallinity. The authors evidenced that samples calcined at higher temperatures are more aggregated with a foamed aspect because of the smallest particle size of the powders. The samples calcined at different temperatures also presented a specific surface area that varied from 66.41 to 37.54 $m^2\ g^{-1}$, and with band gap values from 3.35 to 3.49 eV for the SnO_2-450 and SnO_2-650 samples, respectively.

Curiously, regarding the photocatalytic behavior of the samples prepared by Abdelkader et al. [92], the highest efficiency in the degradation of CR dye (catalyst/CR dye concentration of 0.5 g L^{-1}) was achieved using SnO_2-650 that presented a lower surface area. This sample presented a dye photodegradation efficiency of 61.53% after 100 min under irradiation. The authors pointed out that the highest efficiency observed for this sample is especially due to its greater crystallinity that gives less surface defects as well as particle aggregation. The lower density of surface defects (Sn^{2+} and oxygen vacancies) could reduce recombination of the electron–hole (e^-/h^+) pairs. Because of this fact, the authors proposed the photocatalytic mechanism involved in the CR photodegradation. The reactions mechanism can be represented by Equations (1)–(6). According to the authors, under UVA light, electrons are excited from the VB to the CB of SnO_2 (Equation (1)) and, simultaneously, holes are created in the VB. The photoinduced e^- in the CB can directly reduce Sn^{4+} to Sn^{2+} (Equation (2)). However, as Sn^{4+} can act as a scavenger of e^-, Sn^{2+} can influence the photo-reactivity by altering a e^-/h^+ recombination (Equation (3)). The h^+ in the VB is captured by H_2O generating hydroxyl $^\bullet OH$ radicals (Equation (4)). In addition, according to the band energy position, the authors stated that the h^+ in the VB of SnO_2 (+3.50 eV/NHE) is more positive than that of the H_2O/OH couple (+1.9 eV/NHE), which is required for organic pollutant decomposition $R/R^{\bullet+}$ (+1 V/NHE), indicating that the photoinduced holes in the VB can oxidize the adsorbed CR dye and H_2O molecules on the SnO_2 surface. Thus, the formation of organic cation-radicals ($R^{\bullet+}$) is formed (Equation (5)). As a result, all the $O_2^{\bullet-}$, $^\bullet OH$, and $R^{\bullet+}$ radicals participate in redox reactions responsible for decomposing CR dye (Equation (6)).

$$SnO_2 + UVA(365\ nm) \rightarrow n - SnO_2\ (h^+_{(VB)} + e^-_{(CB)}) \quad (1)$$

$$Sn^{4+} + e^-_{(CB)} \rightarrow Sn^{2+} \quad (2)$$

$$Sn^{2+} + 2O_2 \rightarrow 2O_2^{\bullet-} + Sn^{4+} \quad (3)$$

$$H_2O + h^+_{(VB)} \rightarrow {}^\bullet OH \quad (4)$$

$$R + h^+_{(VB)} \rightarrow R^{\bullet+} \quad (5)$$

$$(O_2^{\bullet-}, {}^\bullet OH, R^{\bullet+}) + \text{CR dye} \rightarrow \text{intermediate products} \rightarrow \text{Dye degradation} \quad (6)$$

Although most studies concerning photocatalytic degradation of dyes using pure SnO_2 have been performed under UV light, some authors investigated the photocatalytic properties of SnO_2 under visible light and sunlight. For instance, Kumar et al. [94] reported the use of SnO_2 particles prepared by a simple, eco-friendly, and low-cost biosynthesis process using guava (*Psidium guajava*) leaf extract in the photodegradation of Reactive yellow 186 (RY186) dye under sunlight. The authors prepared the samples by mixing a 2.1 M $SnCl_4$ solution with the extracts in a ratio of 1:1, and kept under stirring at 60 °C for 4 h, followed by calcination at 400 °C for 4 h to obtain SnO_2 nanoparticles. The authors evidenced that the SnO_2 single-phase nanoparticles with a size of 8–10 nm showed a high photocatalytic efficiency, degrading 90% of RY186 dye in 180 min. For the photocatalysis, a concentration of 1 g L^{-1} of SnO_2 sample was used. According to the authors, superoxide ($O_2^{\bullet-}$) and hydroxyl ($^\bullet OH$) radicals are responsible for the photodegradation of dye. The efficiency of the photocatalyst in the degradation and mineralization of RY186 was confirmed by CO_2 evolution during the photocatalysis, which was analyzed by GC analysis. The authors evidenced the complete mineralization of dye led to CO_2 (0.8 μmol) and H_2O. As the photostability and reusability of the photocatalyst are important aspects, the authors

evaluated them by performing five consecutive photocatalytic cycles. The photoactivity of the catalyst remained about constant even up to five experiments, although gradual losses in activity were expected. It is important to highlight that the use of powdered samples in photocatalysis might be disadvantageous due to the loss in the amount of the catalyst after centrifugation and filtration processes, which leads to a loss in photoactivity. However, the authors reinforced that the synthesized catalyst is easily separable from the solution.

Like Kumar et al. [94], Haq et al. [78] synthesized tin dioxide (SnO_2) nanoparticles by an eco-friendly process using leaves extracts. However, in the study conducted by Haq et al. [78] *Daphne mucronata* leaf extract was used as a capping and reducing agent in order to control particle size and morphology. The authors evaluated the photocatalytic performance of the samples toward Rhodamine 6G (R6G) dye degradation using 0.4 g L^{-1} of the catalyst. For the materials synthesis, a mixture of a 0.003M $SnCl_4 \cdot 5H_2O$ solution with 20mL of the leaf extract was kept under 500 rpm and stirring at 55 °C. A greenish gel was obtained after 40 min and aged for 24 h, which was subsequently washed with hot water, filtered, washed with ethanol, and finally dried at 100 °C for 6 h to obtain a fine, colorless powder. The authors obtained nanoparticle samples with an average particle size of 64 nm and specific surface area around 147 m^2 g^{-1}. A maximum of 99.70% of the dye degradation was observed after 390 min under simulated sunlight. The charge generation and photodegradation mechanism reported by Haq et al. [78] is the same as the one described by Kumar et al. [94] for RY186 dye [94].

Kumar et al. [94] synthesized SnO_2 nanocrystals by a solution-phase growth technique, and the structural, optical, and photocatalytic properties of the nanostructures were investigated. The effects of reaction temperature (180 and 200 °C), time (24 and 30 h), the use of CTAB (CetylTrimethylAmmonium Bromide) surfactant on the particle size, morphology, and band gap energy were evaluated. According to the authors, the SEM images showed that samples synthesized at 180 °C for 24 (Sample 1) and 30 h without the surfactant (Sample 2) presented particles with a rod-like morphology and crystallite size of 17.12 and 26.51 nm, respectively. When the sample was synthesized at 200 °C for 24 h without surfactant (Sample 3), SnO_2 nanostructures with a nanoflower-like morphology, with crystallite size at 28.25 nm were obtained. On the other hand, the samples prepared at 180 (Sample 4) and 200 °C for 24 h with the addition of CTAB (Sample 5) showed particles with a nanosphere-type morphology with sizes of 23.80 and 32.14 nm, respectively. The band gap (*Eg*) values estimated for sample 1 (nanorods), Sample 2 (nanorods), Sample 3 (nanoflowers), Sample 4 (nanospheres), and sample 5 (nanospheres) were 4.05, 3.88, 3.84, 3.95, and 3.76 eV, respectively. The authors associated the variation of the *Eg* values mainly to the temperature and time conditions of which the samples were prepared, that directly affected the particle size and morphology and, therefore, impacted photocatalytic activity of the samples. Despite the wide band gap of the samples, the authors evaluated their photocatalytic activity using 0.5 g L^{-1} of the catalysts in the degradation of Rhodamine B (RB) dye under direct sunlight irradiation. Surprisingly, the authors observed a high photodegradation of dye under sunlight, and the efficiency of the SnO_2 nanostructures was strongly related to the particles' morphology. According to the authors, even presenting a *Eg* = 3.76 eV, sunlight was enough to promote photoexcitation in Sample 5 to degrade 91.7% of the dye after 2 h. As expected, Sample 1 (SnO_2 nanorods with *Eg* = 4.05 eV) displayed the lowest dye degradation efficiency in 2 h (76% of the dye is degraded). The authors established that size, morphology, specific surface area, and dispersion of the catalysts played key role in the photodegradation of the dye.

Assis et al. [58] used a polymeric precursors method to prepare SnO_2 particles at different temperatures (700, 800, and 900 °C). After being prepared, the powders were impregnated in polystyrene foams in order to increase surface area due to the porous characteristic of polystyrene, besides a favoring for the recovery of the material after use. The photocatalytic property of the samples was investigated in the degradation of RhB dye under UV irradiation with a catalyst/dye concentration of 0.4 g L^{-1}. The authors observed, using high-resolution transmission electron microscopy (HRTEM), that the SnO_2 samples

present nanoparticles with sizes ranging between 20 and 80 nm. Moreover, the formation of agglomerates was observed in the samples calcined at higher temperatures (800 and 900 °C). The oxide obtained at lower temperatures presented a smaller particle size and a larger surface area, which resulted in a greater photocatalytic activity, degrading 98.2% of degradation of the rhodamine RhB after 70 min.

A very conventional synthesis procedure for obtaining oxide-based catalysts is the so-called sol-gel method. Thus, Najjar et al. [93] synthesized SnO_2 nanoparticles by a green sol-gel method, using chitosan as a polymerizing agent, and calcined it at different temperatures (500, 700, 800, and 1000 °C). The authors also draw attention to the use of chitosan that may increase particle stability, prevent particles aggregation, and reduce the particles' toxicity. According to the TGA-DTA analysis, the temperature of 700 °C (namely, SnO_2-NPs at 700 °C) proved to be more adequate to prepare the desirable SnO_2 catalyst. The material calcined at this temperature presented a spherical particle morphology with an average size of 10 nm, as observed by TEM analyses. The authors evaluated the photocatalytic properties of SnO_2-NPs at 700 °C toward the photodegradation of Eriochrome black T (EBT), an azo-type anionic dye. The photocatalytic tests were carried out by adding 21.1 mg L^{-1} of the catalyst in 100 mL of EBT dye solution (10^{-5} M) and kept at a constant stirring and UV irradiation (Hg vapor lamp, 500 W) for 270 min. Regarding the photocatalytic activity of the prepared SnO_2-NPs, a photodegradation efficiency of 77% was obtained after 270 min. In order to investigate the best conditions for optimum dye degradation using SnO_2-NPs, Najjar et al. [93] also investigated the influence of the catalyst concentration (8.7, 21.1, and 43.2 mg L^{-1}) and the solution pH (3.5, 5, 7, and 9). The authors observed an increase of the photodegradation rate by increasing the concentration of the photocatalyst from 8.7 to 21.1 mg L^{-1}, decreasing afterwards. According to the authors, this decrease in photocatalytic efficiency of SnO_2-NPs in a higher concentration is due to the fact of accumulation of nanoparticles that lead to a decrease in the generation of reactive radicals, such as hydroxyls ($^{\bullet}OH$). With respect to variation of the solution pH, the highest photodegradation efficiency (77%) was attained at the isoelectric point of SnO_2-NPs at pH 3.5 (Zeta potential = 0 eV). Curiously, the photodegradation of the anionic EBT dye at positive Zeta potential values (at pH 2) was not as expressive as that observed at the isoelectric point of the catalyst.

According to Najjar et al. [93] the general mechanism involved in the dye photodegradation using SnO_2-NPs is summarized by Equations (7)–(12), that are similar to those reactions displayed in Figure 1 for a hypothetical catalyst.

$$SnO_2 + h\nu \rightarrow SnO_2 + (h^+_{(VB)} + e^-_{(CB)}) \quad (7)$$

$$SnO_2\ (h^+_{(CB)}) + H_2O \rightarrow SnO_2 + H^+ + {}^{\bullet}OH \quad (8)$$

$$SnO_2\ (e^-_{(CB)}) + O_2 \rightarrow SnO_2 + {O_2}^{-\bullet} \quad (9)$$

$${O_2}^{-\bullet} + H^+ \rightarrow {HO_2}^{\bullet} \quad (10)$$

$${HO_2}^{\bullet} + H_2O \rightarrow H_2O_2 + {}^{\bullet}OH \quad (11)$$

$$\text{Dye} + {}^{\bullet}OH \rightarrow \text{degradation dye} \quad (12)$$

As the photostability of the catalyst is an important factor for its reuse in consecutive photocatalytic tests, cyclic experiments of EBT photodegradation were carried out for the SnO_2-NPs under the optimal conditions established in the work. Thus, Najjar et al. [93] evidenced that the degradation rate of EBT remained over 74% after five cycles. In addition, using FTIR, XRD, TEM, and FESEM analysis, the authors showed that no visible changes were observed in the samples after the fifth cycle, which confirms the high photostability of the synthesized catalyst.

Recently, Luque et al. [39] synthesized SnO_2 nanoparticles (SnO_2 NPs) by a green synthesis using *Citrus x paradisi* extract as a stabilizing capping agent. There were different concentrations of the extract (1, 2, and 4% in relation to the aqueous medium—SnO_2

NPs-1, 2, and 4%). It is important to highlight that a heating treatment at 400 °C for 1 h was completed to obtain crystallized SnO_2 NPs. The authors obtained crystalline SnO_2 nanoparticles with average sizes of 9.1, 5.1, and 4.7 nm when 1, 2, and 4% of the capping agent was used in the synthesis, respectively. These samples also presented band gap values (*Eg*) of 3.28, 2.77, and 2.69 eV, respectively, which were smaller than those *Eg* values reported by Mahmood et al. [95]. This confirmed the role of this capping agent in controlling the particles' size, as well as in the modification of optical band gap properties of SnO_2 NPs. The photocatalytic properties of the samples were then investigated under both solar and UV irradiation using a SnO_2 NPs/dye concentration of 1.0 g L^{-1}. Furthermore, Methyl orange (MO), Methylene blue (MB) and Rhodamine B (RhB) were used as target dyes. Regarding the photocatalytic efficiency of the SnO_2 NPs, SnO_2 NPs-4% presented the highest efficiency in the degradation of the dyes, degrading 100% of MO after 180 and 20 min under solar and UV irradiation, respectively. In relation to other dyes, SnO_2-NPs-4% degraded 100% of MB and RhB after 60 min under UV irradiation. The efficiency of this photocatalyst in degrading MO, MB, and RhB dyes under these conditions was confirmed by Turnover number (TON) and Turnover frequency (TOF) analysis. The authors associated the superior photocatalytic efficiency of SnO_2-NPs-4% to the smaller particle size, larger surface area, and the increased number of active sites present on the surface when compared to the other samples. Finally, the authors investigated the involvement in the degradation of dyes, and they evidenced that $^{\bullet}OH$ radicals are the main species responsible for degradation.

Apart from the above-mentioned SnO_2-based photocatalysts prepared by various synthesis methods and the experimental conditions, the search for different photocatalytic materials with the desired efficiency is still a challenge. In this context, different authors have prepared SnO_2 catalysts, owing to the flexibility of applications, including photocatalysis. Compared to powdered materials, the use of films in photocatalysis has some advantages, especially for being easily recovered and reused in different batches. For instance, Bezzerouk et al. [80] deposited SnO_2 thin films on glass substrates at 450 °C by an ultrasonic spray pyrolysis technique, and desired polycrystalline SnO_2 films were obtained with a band gap of 3.80 eV, greater than that for bulk SnO_2 (*Eg* = 3.6 eV). The authors evaluated the photocatalytic property of the films toward Methylene blue (MB) degradation under UV-LEDs (340–400 nm, 7 W) and ultrasound (US) transducer (40 KHz). Different degradation processes were investigated, such as: photolysis (UV), photocatalysis (SnO_2 + UV), the sonolysis process (US), and sonocatalysis (SnO_2 + US) as well as sonophotolysis (US + UV) and sono-photocatalysis (SnO_2 + UV + US). Curiously, SnO_2 film did not show meaningful activity in the degradation of MB dye under UV irradiation (photocatalysis). However, when US was employed, a pronounced increase in the dye degradation was observed, reaching to 88.33%, 94.31%, 97.28%, and 98.25% of efficiency when sono-photocatalysis (SnO_2 + UV + US), sonolysis (US), sonophotolysis (US + UV) and sonocatalysis (SnO_2 + US) processes were used, respectively. The authors associated the highest efficiency of dye degradation using sonocatalysis to the production of acoustic cavitation in the water that can favor the dissociation of water and the formation of an important quantity of $^{\bullet}OH$ radicals that participate in the degradation of dye. Finally, the authors associated the lower efficiency of the processes under UV irradiation to the rapid recombination of the electron–holes during SnO_2 photoexcitation. Therefore, authors showed different processes used to improve dye degradation using SnO_2-based material.

As one could see, several methods and experimental conditions were employed to synthesize undoped SnO_2 materials (in powder and film forms) with different characteristics and properties. It has been shown that these characteristics can directly impact the photocatalytic activity toward the degradation of dyes under UV-visible light, as well as under direct or simulated sunlight or even coupled with ultrasound irradiation. A summary of some important works concerning the photocatalytic applications of different undoped SnO_2 materials obtained by different methods is listed in Table 2.

Table 2. Summary of works related to the synthesis of pure SnO_2 materials by different methods and their application as photocatalysts for organic dye degradation.

Catalyst Type	Synthesis Method	Synthesis Conditions (Temperature/Time of Calcination)	Dye Solution Concentration (mg L^{-1})	Photocatalyst Concentration (g L^{-1})	Pollutant *	Irradiation	Efficiency/Time
SnO_2 NPs [94]	Green solution synthesis	400 °C/4 h	40	1.0	RY186	Sunlight	90%/3 h
SnO_2 NPs [90]	Continuous microwave flow synthesis (CMFS)	200 °C/2 h	50	-	MB	UV	93%/4 h
SnO_2 NPs [92]	Sol-gel	650 °C/4 h	20	0.5	CR	UVA	61.53%/1.66 h
SnO_2 NPs [40]	Green solution synthesis	400 °C/1 h	0.75	1.0	MO MB RhB	UV	(MO) 00%/0.33 h (MB) 100%/1 h (RhB) 100%/1 h
SnO_2 NPs [93]	Green sol-gel	700 °C/2 h	4.61	0.21	EBT	UV	77%/4.5 h
SnO_2 NPs [91]	Green solution synthesis using *Tinospora Cordifolia* extracts	400 °C/2 h	20	2.0	RhB	UV	99.9%/0.75 h
SnO_2 NPs [78]	Green solution synthesis	100 °C/6 h	15	0.4	R6G	Simulated sunlight	99.7/6.5 h
SnO_2 microflowers [95]	One-pot hydrothermal	190 °C/24 h	10	1.0	RhB	UV	99%/2 h
SnO_2 nanocrystals [96]	Solution phase growth technique	200 °C/24 h	5	0.5	RhB	UV-visible	91.7%/2 h
SnO_2 NPs [97]	Electrospinning by precursor solution	120 °C/48 h	5	1.33	MO MB	UV	(MO) 92%/4 h (MB) 95%/4 h
SnO_2 nanorods [85]	Chemical precipitation/hydrothermal	550 °C/4 h	20	0.6	MO	UV	52%/1 h
SnO_2 multilayered films [93]	Microwave hydrothermal	800 °C/2 h	10	-	RhB	UV	100%/4 h
SnO_2 thin films [88]	SPD using microscopy	500 °C/6 h	3.99	-	MB MO	UVA/H_2O_2	(MB) 42%/6 h (MO) 26%/6 h
SnO_2 thin films [80]	Ultrasonic spray pyrolysis technique	450 °C	-	-	MB	UV	98%/0.66 h

* Pollutants: RY186—Reactive yellow 186; MB—Methylene blue; MO—Methyl orange; MG—Malachite green; MR—Methylene red; CR—Congo red; RhB—Rhodamine B; R6G—Rhodamine 6G; EBT- Eriochrome Black T.

It is known that, to design an efficient system, photocatalysts usually need to meet some requirements, such as appropriate band gaps for light absorption, effective charge of carriers' separation, and appropriate VB and CB edge potentials. However, it is difficult for pure SnO_2-based photocatalysts to satisfy all of them. In this sense, doping SnO_2 with different cations and the formation of SnO_2-based composites with other materials have attracted interest, as they drive other possibilities of photocatalytic studies. Therefore, discussion of different works concerning the photocatalytic properties of doped SnO_2 and SnO_2-based composite is given in the following sections.

4.2. Doped SnO_2 Photocatalysts

Although pure SnO_2 nanoparticles with a different morphology have shown efficiency in the degradation of dyes under irradiation, different authors have developed strategies to overcome the low photoactivity of SnO_2 under visible light exposure. For instance, doping SnO_2 with different foreign ions has shown to be an efficient way to shorten its band gap and enhance its photoactivity.

Based on this fact, N. Mala et al. [98] synthesized SnO_2 nanoparticles doped with Mg^{2+} + Co^{3+} cations by a low-cost chemical solution method and investigated the antibacterial activity and photocatalytic efficiency toward the degradation of Methylene blue (MB) and Malachite green (MG) dyes. The authors revealed that the samples presented a tetragonal crystalline phase, with an average crystallite size of 24 and 25 nm for pure SnO_2 and SnO_2-Mg:Co, respectively. The authors suggested that this slightl increase of the crystallite size after doping was due to local distortions in the SnO_2 lattice induced by the presence of dopants. A nanorod-like morphology was confirmed through SEM images, with a reduction in the crystal length and in the average diameter after doping. Surprisingly, an increase in the band gap energy estimated for SnO_2 (3.52 eV) and SnO_2-Mg:Co (4.22 eV) was observed. This behavior is attributed to the quantum confinement effect that normally happens when the nanoparticle size decreases. However, no meaningful variation was observed in the particle size for pure and doped SnO_2 samples. Regarding the photocatalytic activity of SnO_2 and SnO_2:Mg:Co nanoparticles, the authors observed that SnO_2 presented an efficiency of 82 and 86%, while SnO_2-Mg:Co displayed 89 and 92% efficiency toward MB and MG dyes degradation, respectively, under visible light after 60 min. The authors explained that three factors are responsible for the increase in the photocatalytic efficiency of doped SnO_2, which are: prevention of the recombination of electron–hole pairs photogenerated by surface defects, generation of greater number of oxidative species ($^{\bullet}OH$, O_2^-, and H_2O_2), and particle size reduction.

Chu et al. [99] synthesized Bi^{3+}-doped SnO_2 by the hydrothermal method at 180 °C for 24 h, with a variation of bismuth molar content (3, 5 and 7%). The Rhodamine B (RhB) and Ciprofloxacin hydrochloride (CIP) were used as target molecules to evaluate the photocatalytic activity of the synthesized materials under simulated sunlight. XRD analysis confirmed the cassiterite tetragonal phase for all the samples, with no secondary phases, confirming that Bi^{3+} is dissolved into the oxide crystal lattice by replacing Sn^{4+} during the synthesis. The Bi^{3+}/Sn^{4+} replacement in SnO_2 was confirmed by HR-TEM, UV–vis DRS, and XPS measurements. The average crystallite sizes decreased as a function of doping from 5.3 nm in SnO_2 to 3.3 nm in Bi-SnO_2(7%). In addition, the band gap (*Eg*) values showed a subtle variation of 3.72, 3.75, and 3.78 eV for Bi-SnO_2(3%), Bi-SnO_2(5%), and Bi-SnO_2(7%) samples, against 3.86 eV for the pure one. The authors state that the introduction of new levels in the band gap of materials can act as a trap center for electron and hole, reducing charge recombination, which is beneficial to improve photocatalytic activity. By using PL spectroscopy, authors confirmed the lower recombination charge rate in the Bi-SnO_2(5%) sample for presenting the lowest PL emission among all samples. Regarding the photocatalytic activity, Bi-SnO_2(5%) showed an efficiency of 98.28% of RhB dye degradation after 100 min and 92.13% of CIP degradation after 90 min under irradiation. The excellent photodegradation efficiency of the doped samples was due to the increase in light absorption, as well as the effective separation and migration of photogenerated

charge carriers. All the results also indicated that there is an ideal amount of Bi^{3+} doping to optimize the mentioned characteristics in order to enhance the SnO_2 material functionality.

Although doped SnO_2 is most prepared in powder, thin films based on doped SnO_2 have also been studied in photocatalysis. For instance, S. Vadivel and G. Rajaraja et al. [84] prepared magnesium-doped SnO_2 films by the chemical bath deposition method, varying Mg^{2+} molar concentrations (1, 5, and 10%). The films were deposited on glass, and after deposition they were annealed at 500 °C for 5 h in air to promote crystallization. From XRD analysis, the tetragonal rutile phase was confirmed in all films. Atomic force microscopy (AFM) images revealed that the surface roughness decreases with increasing dopant concentration. The optical band gap energy for pure SnO_2 was 3.63 eV, decreasing to 3.42 eV for the film doped with 10% Mg. The photocatalytic activities of the films were evaluated by the degradation of Methylene blue (MB) and Rhodamine B (RhB) dyes under UV irradiation. The maximum photodegradation of the dyes was reached for 10% Mg-doped SnO_2 film, degrading 80% of MB and 90% of RhB after 120 min. Fast electron transfer and high efficiency in electron–hole pairs separation led to a significant improvement of photocatalytic activity in the doped sample.

In the work conducted by Haya et al. [82] films of pure SnO_2 and doped with 2, 4, 6, and 8% of Sr^{2+} were prepared by a chemical solution deposition method using the sol-gel method to deposit the solution coating on a glass substrate. The effect of doping on the structural, optical, morphological, and photocatalytic properties of the films were studied. According to the results, the increase in Sr^{2+} doping promotes a decrease in crystallite size and an increase in the lattice distortion. These effects generate a greater number of defects, such as grain boundaries, micro-stresses, and displacements in the thin film lattice. The average crystallite size decreased from 7.61 nm for undoped SnO_2 to 3.80 nm for 8% Sr-SnO_2. It was also observed by UV-visible analysis that the presence of dopants introduced new intermediate levels in the semiconductor band gap (*Eg*), decreasing *Eg* from 3.86 eV for pure SnO_2 film to 3.76 eV for Sr-richer SnO_2 film. Additionally, the morphology of the films was analyzed by AFM, and a smaller grain size was observed for 8% Sr-SnO_2 (4.96 nm). Consequently, it showed the lower surface roughness when compared to the other films. Concerning the photocatalytic activity, the greatest efficiency in the degradation of MB dye under irradiation was attained for 8% Sr-SnO_2 film, which was attributed to smaller grain sizes and surface roughness, as well as the introduction of new energy levels below the conduction band of the pure material, resulting from the Sr doping.

Using a non-conventional method to prepare thin films, Loyola Poul Raj et al. [83] prepared SnO_2 thin films doped with 3 and 6 mol% of Tb^{3+} on a glass substrate by the spray nebulized pyrolysis (NSP) method and calcined them at 400 °C to crystallize the materials. The authors investigated the photocatalytic property of the films in the degradation of MB dye under UV irradiation. According to the authors, doping SnO_2 films with up to 6% of Tb^{3+} cations induces a decrease in the grain size from 80 to 56 nm, and the band gap from 3.51 to 3.36 eV, which directly impacts photocatalysis, as reported by other authors. Indeed, a maximum of 85% of dye degradation was observed after 120 min under UV irradiation using SnO_2 film doped with the 6 mol% Tb^{3+}. Using PL spectroscopy, the authors reveal that Tb doping leads to the creation of more defects that act as reactive sites for catalyzed reactions. As a consequence of the study, the authors concluded that Tb doping favored photocatalytic reactions by reducing particle size, and therefore increasing the surface area and the number of reactive sites on the surface, which allows the dye adsorption. In addition, Tb doping induces a decrease in the band gap of the materials, which favors photo-absorption, aiming to potentialize charge carriers to participate in photocatalytic reactions.

Other studies based on the synthesis of doped SnO_2 catalysts and their applications in the photodegradation of different organic dyes are listed in Table 3.

Table 3. Summary of the studies for doped SnO_2-based photocatalysts applied in the photodegradation of different organic dyes.

Catalyst Type	Synthesis Method	Synthesis Conditions (Temperature/Time of Calcination)	Dye Solution Concentration (mg L^{-1})	Photocatalyst Concentration (g L^{-1})	Pollutant *	Irradiation	Efficiency/Time
SnO_2:$Mg^{2+}Co^{3+}$ NPs [84]	Wet chemical method	550 °C/2 h	-	0.5	MB MG	Near UV	(MB) 89%/1 h (MG) 92%/1 h
SnO_2:Sr^{2+} thin films [82]	Sol–gel method using a dip-coating technique	500 °C/2 h	5	-	MB	UV	37.90%/2 h
SnO_2:Tb^{3+} thin films [83]	Nebulized spray pyrolysis (NSP) technique	400 °C	3.2	-	MB	UV	85%/2.08 h
SnO2:Bi^{3+} quantum dots [99]	One-step hydrothermal	180 °C/24 h	20	1.0	RhB	UV	98.58%/1.66 h
SnO_2:Mg^{2+} thin films [84]	Chemical bath deposition	500 °C/2 h	15	-	MB	UV	(MB) 80%/2 h
SnO_2:Co^{3+} [100]	Chemical solution	400 °C/2 h	60	0.2	MB	UV-visible	95.38%/2 h
SnO_2:Ni^{2+} NPs [101]	Chemical precipitation	410 °C/2 h	5	0.15	BG	UV	97.54%/1.75 h
SnO_2:Zn^{2+} NPs [102]	Combustion	600 °C/8 h	10	1.0	MB MO	UV	1.6%/1 h 40%/1 h
SnO_2:Zr^{4+} NPs [103]	Co-precipitation	200 °C/24 h	20	-	MO	UV	89.6%/3 h
SnO_2:Mn^{2+} nanowires [104]	Co-precipitation	400 °C/4 h	61	1.0	NBB	Solar irradiation	99%/3 h

* Pollutant: BG—Brilliant green; NBB—Naphthol blue black; MB—Methylene blue; MO—Methyl orange; MG—Malachite green; CR—Congo red; RhB—Rhodamine B.

4.3. SnO_2-Based Composite Photocatalysts

As one can see from studies discussed in the sections above, pure and doped SnO_2 particles and films have been well explored. However, SnO_2 has also been combined with other different semiconductors in order to reduce recombination of the photoinduced charge carriers, to therefore improve photocatalytic activity.

Considering this fact, Abdel-Messih et al. [105] synthesized SnO_2/TiO_2 nanoparticles with a spherical mesoporous morphology synthesized by the sol-gel process, using polymethylmethacrylate as a template. The amount of SnO_2 (0–25%) in relation to the mass of pure TiO_2 was varied to obtain composites with different compositions. The samples were calcined at 800 °C for 3 h to ensure complete organic polymer decomposition. In relation to the photocatalytic property of the materials, photodegradation of Rhodamine B (RhB) dye was performed under UV irradiation using a catalyst/dye concentration of 1 g L^{-1}. The photodegradation efficiency of the composites increased with the increase of tin oxide content up to 10% (about 92% of the dye degraded after 3 h). However, the sample with 25 mol% of SnO_2 showed the lowest efficiency, which was attributed to the loss of the titanium anatase phase. The authors concluded that there is an optimal amount of SnO_2 to achieve the maximum efficiency. In addition, the remarkable reduction in particle size by the existence of SnO_2 in the composites enhanced the oxidizing power and extended the photoinduced charge separation, and these were the main reasons for the increase in the catalytic activity of the samples.

Das et al. [36] prepared Sn/SnO_2 nanocomposites by the precipitation method, followed by carbothermal reduction and calcination at 800 °C for 2 h. The authors investigated the photocatalytic property of Sn/SnO_2 composites in the degradation of methylene blue under UV irradiation using a catalyst concentration of 0.5 g L^{-1}. It was found that there was a maximum efficiency of 41% for pure SnO_2 after 210 min under irradiation, while the Sn/SnO_2 composite showed a higher photocatalytic activity of 99%. The highest efficiency observed for the composite was related to the role of Sn on the surface of SnO_2 nanoparticles. As the Fermi energy level of Sn is higher than that observed for SnO_2 due to its lower work function, when metallic Sn is bound on the surface of SnO_2 nanoparticles, electrons migrate from Sn to SnO_2 to reach Fermi-level equilibrium. The effect of the pH solution on the photocatalytic efficiency of the composites was also evaluated. The pH had a direct influence on the photocatalytic process, being the neutral pH favorable for the degradation of MB dye. Finally, the authors investigated the reusability of the composites after three cycles and confirmed that the photocatalyst is stable, but gradual loss in efficiency was observed due to the loss of the material during recovery processes.

Li et al. [85] synthesized carbon-coated, mixed-phase (tetragonal/orthorhombic) SnO_2 (i.e., tetragonal/orthorhombic) nanorods photocatalysts by a combined chemical precipitation and hydrothermal method at 180 °C for 6 h. The SnO_2-C composite with a SnO_2 tetragonal phase was obtained after calcination of the hydrothermal products at 550 °C for 4 h. The photocatalytic activities of the samples were investigated toward the degradation of Methyl orange (MO) dye under UV irradiation using a catalyst/dye concentration of 0.6 g L^{-1}. The as-prepared mixed-phase SnO_2 showed a photodegradation activity of 52% against an efficiency of 39% for pure SnO_2 with a tetragonal phase after 60 min under irradiation, indicating the influence of different phases on the junction formation to tune photocatalytic activity. Coating mixed-phase SnO_2 nanorods with carbon provided a degradation activity of 98%. The tetragonal/orthorhombic-SnO_2 material exhibits very high stability after three cycles, remaining about constant without apparent deactivation. Photocatalytic activity was not primarily attributed to the narrower band gap or visible light absorption tail. By demonstrating that the transfer and separation of photogenerated electron–hole pairs are improved by the introduction of a carbon layer in interparticle space. To understand the photocatalytic mechanism, different scavengers were used in the study—triethanolamine (TEOA), tert-butyl alcohol (TBA), and benzoquinone (BQ). The results indicated that the species h^+, $O_2^{\bullet -}$, and $HO^{\bullet}$ played important roles in the degradation of MO.

Constantino et al. [97] synthesized a porous composite based on SnO_2/cellulose acetate with the electrospinning method and calcined it at 120 °C for 48 h. The photocatalytic activity of the nanocomposites was studied toward the degradation of MO and MB dyes under UV irradiation using a catalyst/dye concentration of 1.3 g L^{-1}. The photocatalytic efficiency of SnO_2/cellulose was approximately 92% of MO degradation after 210 min and 95% of MB degradation after 240 min. It is worth mentioning that the photodegradation process did not alter the average diameter and morphology of the fibers as well as their surface chemistry. From TOC analysis, the authors evidenced that only 54% and 79% of MO and MB dye are mineralized after the photocatalytic process. However, presence of other compounds as by-product of dye degradation was confirmed by LC–MS.

Silva et al. [37] synthesized spherical nanoparticles and microrods of Ag_3PO_4/SnO_2 composites, by the in situ coprecipitation method, with various molar ratios of 5, 10, 15, and 20% of SnO_2 in relation to the mass of pure Ag_3PO_4, followed by calcination at 350 °C for 2 h. The photocatalytic performance of the samples was investigated by the degradation of Rhodamine B (RhB) dye under visible light irradiation using a catalyst/dye concentration of 0.6 g L^{-1}. The authors observed superior photocatalytic activity for all the composites when compared to pure Ag_3PO_4. The authors evidenced that the excess of SnO_2 damaged the interfacial contact between the Ag_3PO_4 and SnO_2, which was due to the high degree of particle agglomeration. The photocatalytic mechanism involved in the photodegradation of the dye was also investigated for pure Ag_3PO_4 and Ag_3PO_4/SnO_2-15%. It has been confirmed that the photogenerated holes participated in the direct degradation of RhB when Ag_3PO_4 was a photocatalyst. On the other hand, there was a significant participation of $O_2^{\bullet -}$ radicals when Ag_3PO_4/SnO_2-15% is used. The highest photodegradation efficiency presented by the Ag_3PO_4/SnO_2-15% composite was confirmed by total organic carbon (TOC) analysis. Reusability tests were also performed for Ag_3PO_4/SnO_2-15% and a loss of 43.2% of its photocatalytic efficiency was observed after the third cycle, which was similar to that observed for pure Ag_3PO_4. Using the X-ray diffraction technique, the presence of Ag in the composition of the samples was observed after the photocatalysts were used in photocatalysis.

Apart from the above-mentioned studies performed using composite particles, SnO_2-based composite photocatalysts have also been explored as films. For instance, porous SnO_2/TiO_2 films were prepared using Ar-assisted, modified thermal evaporation, followed by the atomic layer deposition (ALD) technique at 300 °C in the reaction chamber [62]. To prepare SnO_2/TiO_2 films, TiO_2 layers were deposited on porous SnO_2 nanofoam, with those previous deposited on 2 × 2 cm^2 Si (100) wafers or ITO substrates, with variation in deposition cycles of TiO_2 (10, 25, 50, and 100 cycles) by ALD. The samples were denoted SnO_2/TiO_2-10, SnO_2/TiO_2-25, SnO_2/TiO_2-50, and SnO_2/TiO_2-100, respectively. After the TiO_2 deposition, the material was calcined at 700 °C for 1 h. The photocatalytic properties of the films were evaluated by the degradation of MB at a concentration of 1.2 mg L^{-1} under UV irradiation. The nanofoam heterostructures showed higher photocatalytic activity when compared to the porous SnO_2 nanofoam. SnO_2/TiO_2-50 nanofoam, which exhibited the highest efficiency, reached to 99% of MB degradation after 300 min. The authors correlated this fact to being due to a synergistic effect occurring between SnO_2 and TiO_2, and due to the sparse deposition of the TiO_2 layer on porous SnO_2. Separation of charge carriers due to the potential difference between SnO_2 and TiO_2 increases the lifetime of the charge and improves the interfacial charge transfer to the species adsorbed on the surface. This phenomenon, along with the strong oxidant $^{\bullet}OH$ radicals formed in the VB of the TiO_2 layer, improves photocatalytic efficiency of the SnO_2/TiO_2 heterostructure.

Other important works reporting the activity of SnO_2-based composite photocatalysts for the degradation of dyes are summarized in Table 4.

Table 4. SnO_2-based composites formed with different semiconductors for photodegradation of organic dyes.

Catalyst Type	Synthesis Method	Synthesis Conditions (Temperature/Time of Calcination)	Dye Solution Concentration (mg L^{-1})	Photocatalyst Concentration (mg L^{-1})	Pollutant *	Irradiation	Efficiency/Time
CrO_4-SnO_2 spherical NPs [106]	Coprecipitation	150, 300 and 450 °C/3 h	1×10^{-4} mol L^{-1}	1.6 g L^{-1}	TB	Sunlight	80%/1 h
g-C_3N_4/SnO_2 nanosheets decorated with NPs [107]	Microwave-assisted hydrothermal method	550 °C/2 h	10 mg L^{-1}	0.5 g L^{-1}	RhB	UV and visible lights	100%/4 h (UV) and 98.5% (visible light)
Zn_2SnO_4–SnO_4 and Zn_2SnO_4–Sn spherical NPs [108]	Solid state reaction	800 °C/1 h	20 mg L^{-1}	0.2 g L^{-1}	MB	UV	92%/2 h
Polyaniline SnO_2 nanoneedles and nanograins [109]	Chemical oxidation polymerization method using aniline monomer	500 °C/2 h	50 mg L^{-1}	1 g L^{-1}	RY	UV	96%/1 h
ZnO-SnO_2 thin films [81]	Sol-gel	550 °C/1 h	16 mg L^{-1}	-	MeG	UV	42%/45 min
ZnO-SnO_2/NPs hexagonal nanopillar [110]	Sol-gel	600 °C/2 h	10 mg L^{-1}	0.025 g L^{-1}	MO MB CR	UV	91.78%/3 h (MO) 93.21%/3 h (MB) 85.14%/3 h (CR)
$CuCr_2O_4$/SnO_2 [111]	Sol-gel/solid state reaction	900 °C/6 h and 600 °C	15 mg L^{-1}	1 g L^{-1}	CV	Sunlight	100%/1.5 h
SnO_2/GO spherical NPs [112]	Sonochemical method	180 °C/6 h and 100 °C/6 h	1×10^{-5} mol L^{-1}	0.5 g L^{-1}	RhB TDW	Sunlight	95%/2 h (RhB) 100%/2.5 h (TDW)
SnO_2/Zn_2SnO_4 cube-like NPs [113]	Hydrothermal	150 °C/12 h and 700 °C/2 h	10^{-5} mol L^{-1}	1 g L^{-1}	MB MO EBT	Simulated sunlight	97.1%/2.5 h (MB) 93.7%/3 h (MO) 87.9%/3.5 h (EBT)
SnO_2-MoS_2 spherical NPs [114]	Sonochemical liquid exfoliation method	80 °C/2 h	100 ppm	1 mL of SnO_2-MoS_2 added in 50 mL of dye solution	MR MB	Visible light	94.0%/2 h (MR) 58.5%/2 h (MB)
SnO_2-WO_3 NPs [115]	Green combustion method	500 °C/1 h	5 ppm	0.8 g L^{-1}	MB	Visible light	70%/3 h

* Pollutant: CV—Crystal violet; CR—Congo red; EBT—Eriochrome black T; MB—Methylene blue; MO—Methyl orange; MeG—Methyl green; MR—Methylene red; RhB—Rhodamine B; RY—Remazol yellow; TB—Trypan Blue; TDW—Textile dye wastewater.

Most of the authors reported that the number of materials for the formation of the SnO_2 with a different particle size and morphology, besides doped SnO_2 with an appropriate amount and type of dopant, and also the formation of the composite with SnO_2, plays an important role in improving the photocatalytic activity of the SnO_2 material. In relation to composites, the excess of both species can be harmful to the contact surface between the phases, mainly due to the high degree of particle agglomeration. Tests using scavengers, such as p-benzoquinone (BZ, $C_6H_4O_2$), isopropanol (ISO, $(CH_3)_2CHOH$), and ammonium oxalate monohydrate (AO, $(NH_4)_2C_2O_4 \cdot H_2O$) indicate $^{\bullet}OH$ is the main species in most photocatalytic mechanisms. However, to obtain more insights about the photocatalytic mechanism involved in composite materials, we seek to understand the charge transfer between the phases from the band structures of each individual material. Structural and electronic defects can also generate energy levels between the VB and CB, and, therefore, modify the photocatalytic mechanism of composites. The creation of different interfaces between the phases may reduce charge carriers' recombination, leading to the formation of a great number of free radicals to improve photocatalysis. In addition, several other parameters can impact the photocatalytic efficiency of composites, such as phase composition, surface area, morphology, particle size, pore structure, electron–hole recombination rate, and band gap energy of the individual components. Some authors showed that the high surface area and the presence of pores are more effective parameters that affect dye degradation since the existence of several active sites, responsible for the adsorption of molecules, is crucial for the photocatalysis to occur.

Based on the findings above, it can be concluded that to design a new photocatalytic material with specific characteristic, one has to consider optimizing type and amount of dopants and interface characteristics between materials, or even the nature of the desired product (powder, film, etc.), besides the microstructure of the material (particle size and morphology), and by a choice of specific synthesis methodology and appropriate experimental conditions.

5. Conclusions and Final Remarks

From this review work, it was possible to evaluate the importance of synthesis methods and experimental parameters in obtaining tin-oxide-based materials with high performance in heterogenous photocatalysis of persistent organic pollutants, more specifically, organic dyes. The search for new materials and methodologies that provide efficient results for the remediation of such pollutants has been one of the great challenges for the scientific community. Among the studied promising materials, SnO_2 has shown excellent results as a catalyst in heterogeneous photocatalysis processes due to its intrinsic characteristics, which have been responsible for the material's conductivity, optical and electrical properties, and high thermal stability. As a consequence of the choice of the synthesis method and experimental conditions, it was possible to evidence different morphology, particle size, surface area, structural modifications, optical bandgap energy, and surface and bulk defects, and, therefore, obtain excellent results in the application of pure and modified SnO_2 toward the degradation of persistent organic pollutants (POPs). In general, SnO_2-based photocatalysts have shown promising efficiency for degrading a series of different organic dyes.

Considering pure SnO_2 catalysts, synthesis conditions may especially influence particle size and morphology, specific surface area, crystallinity, and the presence of electronic defects on surface and bulk of the materials, which are important parameters to change photocatalytic efficiency under both UV and visible irradiation. With respect to doped SnO_2, the type and number of dopants may introduce different intermediate levels within the gap, decreasing band gap energy to improve the photo-absorption in visible light. Finally, it has been demonstrated that the composite formed with SnO_2 is responsible for band structure alignment and improvement of charge separation that led to an increased photocatalytic activity when compared to the individual components. It is still important to highlight that the study of the reaction mechanism involved in the dye degradation is an

important aspect, which allows the design of new and efficient SnO_2-based photocatalysts, and an understanding of their laminations in order to use them in practical devices.

Author Contributions: Conceptualization, M.C.F.A. and A.L.M.d.O.; methodology, J.L.A.d.N., A.L.M.d.O. and M.C.F.A.; validation, A.L.M.d.O. and M.C.F.A.; investigation, J.L.A.d.N.; formal analysis, J.L.A.d.N., L.C., A.L.M.d.O. and M.C.F.A.; data curation: J.L.A.d.N.; writing—original draft preparation, J.L.A.d.N.; writing—review and editing, L.C., A.L.M.d.O. and M.C.F.A.; visualization, I.M.G.d.S.; supervision, A.L.M.d.O. and M.C.F.A.; project administration, M.C.F.A. All authors have read and agreed to the published version of the manuscript.

Funding: This research was funded by CAPES-Brazil (Grant 88887.497404/2020-00).

Institutional Review Board Statement: Not applicable.

Informed Consent Statement: Not applicable.

Acknowledgments: The authors thank PRPGP/UEPB, PPGQ/UEPB and FAPESQ/PRONEX, for financial support. A.L.M.d.O thanks CAPES-Brazil for the PNPD funding (Grant 88882.317938/2019-01).

Conflicts of Interest: The authors declare that they have no conflict of interest regarding the publication of this article, financial and/or otherwise.

References

1. Anastopoulos, I.; Pashalidis, I.; Orfanos, A.G.; Manariotis, I.D.; Tatarchuk, T.; Sellaoui, L.; Bonilla-petriciolet, A.; Mittal, A.; Núnez-delgado, A. Removal of caffeine, nicotine and amoxicillin from (waste)waters by various adsorbents. A review. *J. Environ. Manag.* **2020**, *261*, 110236. [CrossRef] [PubMed]
2. Beltrame, T.F.; Lhamby, A.R.; Beltrame, A. Wastewater, solid waste and environmental education: A discussion about the subject. *Rev. Eletrônica Gestão Educ. Tecnol. Ambient.* **2016**, *20*, 351–362.
3. Kurade, M.B.; Há, Y.; Xiong, J.; Govindwar, S.P.; Jang, M.; Jeon, B. Phytoremediation as a green biotechnology tool for emerging environmental pollution: A step forward towards sustainable rehabilitation of the environment. *Chem. Eng. J.* **2021**, *415*, 129040. [CrossRef]
4. Tao, Y.; Wu, Y.; Zhou, J.; Wu, M.; Wang, S.; Zhang, L.; Xu, C. How to realize the effect of air pollution control? A hybrid decision framework under the fuzzy environment. *J. Clean. Prod.* **2021**, *305*, 127093. [CrossRef]
5. Shi, Z.; She, Z.; Chiu, Y.; Shijiong, Q.S.; Zhang, L. Assessment and improvement analysis of economic production, water pollution, and sewage treatment efficiency in China. *Socio-Econ. Plan. Sci.* **2021**, *74*, 100956. [CrossRef]
6. Kim, A.Y.; Park, J.B.; Woo, M.S.; Lee, S.Y.; Kim, H.Y.; Yoo, Y.H. Review: Persistent Organic Pollutant-Mediated Insulin Resistance. *Int. J. Environ. Res. Pub. Health* **2019**, *16*, 448. [CrossRef]
7. Tyutikov, S.F. Migration and Biogeochemical Indication of Persistent Organic Pollutants. *Geochem. Int.* **2018**, *56*, 1028–1035. [CrossRef]
8. Arthur, R.B.; Ahern, J.C.; Patterson, H.H. Review Application of BiOX Photocatalysts in Remediation of Persistent Organic Pollutants. *Catalysts* **2018**, *8*, 604. [CrossRef]
9. Li, C.; Yanga, L.; Shic, M.; Liu, G. Persistent organic pollutants in typical lake ecosystems. *Ecotoxicol. Environ. Saf.* **2019**, *180*, 668–678. [CrossRef]
10. Mansouri, E.H.; Reggabi, M. Association between type 2 diabetes and exposure to chlorinated persistent organic pollutants in Algeria: A case-control study. *Chemosphere* **2021**, *264*, 128596. [CrossRef]
11. Ulutaş, O.K.; Çok, I.; Darendeliler, F.; Aydin, B.; Çoban, A.; Henkelmann, B.; Schramm, K. Blood concentrations and risk assessment of persistent organochlorine compounds in newborn boys in Turkey. *A pilot study. Environ. Sci. Pollut. Res.* **2015**, *22*, 19896–19904. [CrossRef] [PubMed]
12. Nascimento, F.P.; Kuno, R.; Lemes, V.G.R.; Kussumi, T.A.; Nakano, V.E.; Rocha, S.B.; Oliveira, M.C.C.; Kimura, I.A.; Gouveia, N. Organochlorine pesticides levels and associated factors in a group of blood donors in São Paulo, Brazil. *Environ. Monit. Assess.* **2017**, *189*, 380. [CrossRef] [PubMed]
13. Stockholm Convention Secretariat United Nations Environment. *An Introduction to the Chemicals Added to the Stockholm Convention as Persistent Organic Pollutants by the Conference of the Parties*; International Environmental House: Vernier, Switzerland, 2017; pp. 2–25.
14. Varakina, Y.; Lahmanov, D.; Aksenov, A.; Trofimova, A.; Korobitsyna, R.; Belova, N.; Sobolev, N.; Kotsur, D.; Sorokina, T.; Grjibovsk, A.M.; et al. Concentrations of Persistent Organic Pollutants in Women's Serum in the European Arctic Russia. *Toxics* **2021**, *9*, 6. [CrossRef] [PubMed]
15. Wagner, M.; Lin, K.A.; Oh, W.; Lisak, G. Metal-organic frameworks for pesticidal persistent organic pollutants detection and adsorption—A mini review. *J. Hazard. Mater.* **2021**, *413*, 125325. [CrossRef]

16. Wang, S.; Hu, C.; Lu, A.; Wang, Y.; Cao, L.; Wu, W.; Li, H.; Wu, M.; Yan, C. Association between prenatal exposure to persistent organic pollutants and neurodevelopment in early life: A mother-child cohort (Shanghai, China). *Ecotoxicol. Environ. Saf.* **2021**, *208*, 111479. [CrossRef]
17. Chen, Y.; Zhi, D.; Zhou, Y.; Huang, A.; Wu, S.; Yao, B.; Tang, Y.; Sun, C. Electrokinetic techniques, their enhancement techniques and composite techniques with other processes for persistent organic pollutants remediation in soil: A review. *J. Ind. Eng. Chem.* **2021**, *97*, 163–172. [CrossRef]
18. Junior, J.C.A.P.; Albuquerque, L.S.; Delfino, N.M.; Muniz, E.P.; Rocha, S.M.S.; Porto, P.S.S. Treatment of synthetic methylene blue dye effluent by electrofloculation. *Braz. J. Prod. Eng.* **2017**, *3*, 105–113.
19. Li, M.; Zhao, H.; Lu, Z. Porphyrin-based porous organic polymer, Py-POP, as a multifunctional platform for efficient selective adsorption and photocatalytic degradation of cationic dyes. *Microporous Mesoporous Mater.* **2020**, *292*, 109774. [CrossRef]
20. Zhao, L.; Houb, H.; Iwasaki, K.; Terada, A.; Hosomi, M. Utilization of recycled charcoal as a thermal source and adsorbent for the treatment of PCDD/Fs contaminated sediment. *J. Hazard. Mater.* **2012**, *225*, 182–188. [CrossRef]
21. Titchou, F.E.; Zazou, H.; Afanga, H.; Gaayda, J.E.; Akbour, R.A.; Hamdani, M. Review Removal of Persistent Organic Pollutants (POPs) from water and wastewater by adsorption and electrocoagulation process. *Groundw. Sustain. Dev.* **2021**, *13*, 100575. [CrossRef]
22. Ji, S.; Yang, Y.; Zhou, Z.; Li, X.; Liu, Y. Photocatalysis-Fenton of Fe-doped g-C3N4 catalyst and its excellent degradation performance towards RhB. *J. Water Process Eng.* **2021**, *40*, 101804. [CrossRef]
23. Ajmal, A.; Majeedb, I.; Malika, R.N.; Iqbal, M.; Nadeemb, M.A.; Hussain, I.; Yousaf, S.; Mustafa, G.; Zafara, M.I.; Nadeem, M.A. Photocatalytic degradation of textile dyes on Cu_2O CuO/TiO_2 anatase powders. *J. Environ. Chem. Eng.* **2016**, *4*, 2138–2146. [CrossRef]
24. Waki, M.; Shirai, S.; Yamanaka, K.; Maegawa, Y.; Inagaki, S. Heterogeneous water oxidation photocatalysis based on periodic mesoporous organosilica immobilizing a tris(2,20-bipyridine)ruthenium sensitizer. *RSC Adv.* **2020**, *10*, 13960. [CrossRef]
25. Lima, A.S.; Rocha, R.D.C.; Pereira, E.C.; Sikora, M.S. Photodegradation of Ciprofoxacin antibiotic over TiO_2 grown by PEO: Ecotoxicity response in *Lactuca sativa* L. and Lemna minor. *Int. J. Environ. Sci. Technol.* **2021**, *19*, 2771–2780. [CrossRef]
26. Araújo, K.S.; Antonelli, R.; Gaydeczka, B.; Granato, A.C.; Malpass, G.R.P. Processos oxidativos avançados: Uma revisão de fundamentos e aplicações no tratamento de águas residuais urbanas e efluentes industriais. *Rev. Ambient. Água* **2016**, *11*, 387–401.
27. Honorio, I.M.C.; Santos, M.V.B.; Filho, E.C.S.; Osajima, J.A.; Maia, A.S.; Santos, I.M.G. Alkaline earth stannates applied in photocatalysis: Prospection and review of literature. *Cerâmica* **2018**, *64*, 559–569. [CrossRef]
28. Cornejo, O.M.; Murrieta, M.F.; Castañeda, L.F.; Nava, J.L. Characterization of the reaction environment in flow reactors fitted with BDD electrodes for use in electrochemical advanced oxidation processes: A critical review. *Electrochim. Acta* **2020**, *331*, 135373. [CrossRef]
29. Moradi, M.; Vasseghian, Y.; Khataee, A.; Kobya, M.; Arabzade, H.; Dragoi, E. Service life and stability of electrodes applied in electrochemical advanced oxidation processes: A comprehensive review. *J. Ind. Eng. Chem.* **2020**, *87*, 18–39. [CrossRef]
30. Honorio, L.M.C.; Oliveira, A.L.M.; Silva-Filho, E.C.; Osajima, J.A.; Hakki, A.; Macphee, D.E.; Santos, I.M.G. Supporting the photocatalysts on ZrO_2: An effective way to enhance the photocatalytic activity of $SrSnO_3$. *Appl. Surf. Sci.* **2020**, *528*, 146991. [CrossRef]
31. Sun, H.; Qin, P.; Wu, Z.; Liao, C.; Guo, J.; Luo, S.; Chai, Y. Visible light-driven photocatalytic degradation of organic pollutants by a novel Ag_3VO_4/Ag_2CO_3 pen heterojunction photocatalyst: Mechanistic insight and degradation pathways. *J. Alloys Compd.* **2020**, *834*, 155211. [CrossRef]
32. Riente, P.; Fianchini, M.; Llanes, P.; Pericàs, M.A.; Noël, T. Shedding light on the nature of the catalytically active species in photocatalytic reactions using Bi_2O_3 semiconductor. *Nat. Commun.* **2021**, *12*, 625. [CrossRef] [PubMed]
33. Hu, W.; Quang, N.D.; Majumder, S.; Jeong, M.J.; Park, J.H.; Cho, Y.J.; Kim, S.B.; Lee, K.; Kim, D.; Chang, H.S. Three-dimensional nanoporous SnO_2/CdS heterojunction for high-performance photoelectrochemical water splitting. *Appl. Surf. Sci.* **2021**, *560*, 149904. [CrossRef]
34. Li, Y.; Wang, J.; Sun, H.; Hua, W.; Liu, X. Heterostructured SnS_2/SnO_2 nanotubes with enhanced charge separation and excellent photocatalytic hydrogen production. *Int. J. Hydrog. Energy* **2018**, *43*, 14121–14129. [CrossRef]
35. Chen, S.; Yang, J.; Wu, J. Three-Dimensional Undoped Crystalline SnO2 Nanodendrite Arrays Enable Efficient Charge Separation in $BiVO_4/SnO_2$ Heterojunction Photoanodes for Photoelectrochemical Water Splitting. *ACS Appl. Energy Mater.* **2018**, *1*, 2143–2149. [CrossRef]
36. Das, O.R.; Uddin, M.T.; Rahman, M.M.; Bhoumick, M.C. Highly active carbon supported Sn/SnO_2 photocatalysts for degrading organic dyes. *J. Phys.* **2018**, *1086*, 012011. [CrossRef]
37. Silva, G.N.; Martins, T.A.; Nogueira, I.C.; Santos, R.K.; Li, M.S.; Longo, E.; Botelho, G. Synthesis of Ag_3PO_4/SnO_2 composite photocatalyst for improvements in photocatalytic activity under visible light. *Mater. Sci. Semicond. Process.* **2021**, *135*, 106064. [CrossRef]
38. Xua, L.; Xiana, F.; Zhanga, Y.; Wang, W.; Qiua, K.; Xu, J. Synthesis of ZnO-decorated SnO_2 nanopowder with enhanced photocatalytic performance. *Opt. Int. J. Light Electron. Opt.* **2019**, *194*, 162965. [CrossRef]
39. Luque, P.A.; Garrafa-Galvez, H.E.; Nava, O.; Olivas, A.; Martínez-Rosas, M.E.; Vilchis-Nestor, A.R.; Villegas-Fuentes, A.; Chinchillas-Chinchillas, M.J. Efficient sunlight and UV photocatalytic degradation of Methyl Orange, Methylene Blue and Rhodamine B, using Citrus×paradisi synthesized SnO_2 semiconductor nanoparticles. *Ceram. Int.* **2021**, *5*, 91. [CrossRef]

40. Santos, J.E.L.; Moura, D.C.; Cerro-López, M.; Quiroz, M.A.; Martínez-Huitle, C.A. Electro- and photo-electrooxidation of 2,4,5-trichlorophenoxiacetic acid (2,4,5-T) in aqueous media with PbO_2, Sb-doped SnO_2, BDD and TiO_2-NTs anodes: A comparative study. *J. Electroanal. Chem.* **2020**, *873*, 114438. [CrossRef]
41. La Fourni'ere, E.M.; Meichtry, J.M.; Gautier, E.A.; Leyva, A.G.; Litter, M.I. Treatment of ethylmercury chloride by heterogeneous photocatalysis with TiO_2. *J. Photochem. Photobiol. A Chem.* **2021**, *411*, 113205. [CrossRef]
42. Furtado, R.X.S.; Sabatini, C.A.; Zaiat, M.; Azevedo, E.B. Perfluorooctane sulfonic acid (PFOS) degradation by optimized heterogeneous photocatalysis (TiO_2/UV) using the response surface methodology (RSM). *J. Water Process Eng.* **2021**, *41*, 10198.
43. Yanga, D.; Gondalb, M.A.; Yamani, Z.H.; Baig, U.; Qiao, Q.; Liua, G.; Xud, Q.; Xiange, D.; Maof, J.; Shen, K. 532 nm nanosecond pulse laser triggered synthesis of ZnO_2 nanoparticles via a fast ablation technique in liquid and their photocatalytic performance. *Mater. Sci. Semicond. Process.* **2017**, *57*, 124–131. [CrossRef]
44. Khatri, A.; Rana, P.S. Visible light assisted photocatalysis of Methylene Blue and Rose Bengal dyes by iron doped NiO nanoparticles prepared via chemical co-precipitation. *Phys. B Phys. Condens. Matter.* **2020**, *579*, 411905. [CrossRef]
45. Mohite, S.V.; Ganbavle, V.V.; Rajpure, K.Y. Photoelectrocatalytic activity of immobilized Yb doped WO_3 photocatalyst for degradation of methyl orange dye. *J. Energy Chem.* **2017**, *26*, 440–447. [CrossRef]
46. Omrani, N.; Nezamzadeh-Ejhieh, A. $BiVO_4$/WO_3 nano-composite: Characterization and designing the experiments in photodegradation of sulfasalazine. *Environ. Sci. Pollut. Res.* **2020**, *27*, 44292–44305. [CrossRef]
47. Al-Hamdi, A.M.; Rinner, U.; Sillanpää, M. Tin dioxide as a photocatalyst for water treatment: A review. *Process Saf. Environ. Prot.* **2017**, *107*, 190–205. [CrossRef]
48. Sun, C.; Yang, J.; Xu, M.; Cui, Y.; Ren, W.; Zhang, J.; Zhao, H.; Liang, B. Recent intensification strategies of SnO_2-based photocatalysts: A review. *Chem. Eng. J.* **2022**, *427*, 131564. [CrossRef]
49. Lavanya, N.; Fazio, E.; Neri, F.; Bonavita, A.; Leonardi, S.G.; Neri, G.; Sekar, C. Simulta neous electrochemical determination of epinephrine and uric acid in the presence of ascorbic acid using SnO_2/graphene nanocomposite modified glassy carbon electrode. *Sens. Actuators B Chem.* **2015**, *221*, 1412–1422. [CrossRef]
50. Sakthiraj, K.; Balachandrakumar, K. Influence of Ti addition on the room temperature ferromagnetism of tin oxide (SnO_2) nanocrystal. *J. Magn. Magn. Mater.* **2015**, *395*, 205–212. [CrossRef]
51. Xiong, L.; Guo, Y.; Wen, J.; Liu, H.; Yang, G.; Qin, P.; Fang, G. Review on the Application of SnO_2 in Perovskite Solar Cells. *Adv. Funct. Mater.* **2018**, *28*, 1802757. [CrossRef]
52. Mouly, T.A.; Toms, L.L. Breast cancer and persistent organic pollutants (excluding DDT): A systematic literature review. *Environ. Sci. Pollut. Res.* **2016**, *23*, 22385–22407. [CrossRef] [PubMed]
53. Gopinath, K.P.; Madhav, N.V.; Krishnan, A.; Malolan, R.; Rangarajan, G. Present applications of titanium dioxide for the photocatalytic removal of pollutants from water: A review. *J. Environ. Manag.* **2020**, *270*, 110906. [CrossRef] [PubMed]
54. Tang, S.H.; Zaini, M.A.A. Isotherm studies of malachite green removal by yarn processing sludge-based activated carbon. *Chem. Didact. Ecol. Metrol.* **2019**, *24*, 127–134. [CrossRef]
55. Adithya, S.; Jayaraman, R.S.; Krishnan, A.; Malolan, R.; Gopinath, K.P.; Arun, J.; Kim, W.; Govarthanan, M. A critical review on the formation, fate and degradation of the persistent organic pollutant hexachlorocyclohexane in water systems and waste streams. *Chemosphere* **2021**, *271*, 129866. [CrossRef]
56. Bilal, M.; Adeel, M.; Rasheed, T.; Zhao, Y.; Iqbal, H.M.N. Emerging contaminants of high concern and their enzyme-assisted biodegradation—A review. *Environ. Int.* **2019**, *124*, 336–353. [CrossRef]
57. Hernandez-Vargas, G.; Sosa-Hernández, J.E.; Hernandez, S.; Villalba-Rodríguez, A.M.; Parra-Saldivar, R.; Iqbal, H.M.N. Electrochemical biosensors: A solution to pollution detection with reference to environmental contaminants. *Biosensors* **2018**, *8*, 29. [CrossRef]
58. Assis, G.C.; Skovroinski, E.; Leite, V.D.; Rodrigues, M.O.; Galembeck, A.; Alves, M.C.F.; Eastoe, J.; Oliveira, R.J. Conversion of "Waste Plastic" into Photocatalytic Nanofoams for Environmental Remediation. *Appl. Mater. Interfaces* **2018**, *10*, 8077–8085. [CrossRef]
59. Aziz, A.; Ali, N.; Khan, A.; Bilal, M.; Malik, S.; Khan, H. Chitosan-zinc sulfide nanoparticles, characterization and their photocatalytic degradation efficiency for azo dyes. *Int. J. Biol. Macromol.* **2020**, *153*, 502–512. [CrossRef]
60. Rawat, D.; Mishra, V.; Sharma, R. Detoxification of azo dyes in the context of environmental processes. *Chemosphere* **2016**, *155*, 591–605. [CrossRef]
61. Chu, D.; Zhu, S.; Wang, L.; Wang, G.; Zhang, N. Hydrothermal synthesis of hierarchical flower-like Zn-doped SnO_2 architectures with enhanced photocatalytic activity. *Mater. Lett.* **2018**, *224*, 92–95. [CrossRef]
62. Kim, S.; Kwang, H.-K.C.; Kim, B.; Hyun-Jong, K.; Lee, H.-N.; Park, T.J.; Park, Y.M. Highly Porous SnO_2/TiO_2 Heterojunction Thin-Film Photocatalyst Using Gas-Flow Thermal Evaporation and Atomic Layer Deposition. *Catalysts* **2021**, *11*, 1144. [CrossRef]
63. Ono, S. High-pressure phase transitions in SnO_2. *J. Appl. Phys.* **2005**, *97*, 073523. [CrossRef]
64. Lian, Y.; Huang, X.; Yu, J.; Tang, T.B.; Zhang, W.; Gu, M. Characterization of scrutinyite SnO_2 and investigation of the transformation with 119Sn NMR and complex impedance method. *AIP Adv.* **2018**, *8*, 125226. [CrossRef]
65. Lin, S.S.; Tsai, Y.; Bai, K. Structural and physical properties of tin oxide thin films for optoelectronic applications. *Appl. Surf. Sci.* **2016**, *380*, 203–209. [CrossRef]

66. Feng, B.; Feng, Y.; Qin, J.; Wang, Z.; Zhang, Y.; Du, F.; Zhao, Y.; Wei, J. Self-template synthesis of spherical mesoporous tin dioxide from tin-polyphenol-formaldehyde polymers for conductometric ethanol gas sensing. *Sens. Actuators B Chem.* **2021**, *341*, 12995. [CrossRef]
67. Noha, M.F.M.; Soha, M.F.; Tehb, C.H.; Lim, E.L.; Yap, C.C.; Ibrahima, M.A.; Ludina, N.A.; Teridi, M.A.M. Effect of temperature on the properties of SnO_2 layer fabricated via AACVD and its application in photoelectrochemical cells and organic photovoltaic devices. *Sol. Energy* **2017**, *158*, 474–482. [CrossRef]
68. Das, M.; Roy, S. Preparation, Characterization and Properties of Newly Synthesized SnO_2-Polycarbazole Nanocomposite via Room Temperature Solution Phase Synthesis Process. *Mater. Today Proc.* **2019**, *18*, 5438–5446. [CrossRef]
69. Muthusamy, S.; Charles, J. In situ synthesis of ternary prussian blue, hierarchical SnO_2 and polypyrrole by chemical oxidative polymerization and their sensing properties to volatile organic compounds. *Optik* **2021**, *241*, 166968. [CrossRef]
70. Mallik, A.; Roy, I.; Chalapathi, D.; Narayana, C.; Das, T.D.; Bhattacharya, A.; Bera, S.; Bhattacharya, S.; De, S.; Das, B.; et al. Single step synthesis of reduced graphene oxide/SnO_2 nanocomposites for potential optical and semiconductor applications. *Mater. Sci. Eng. B* **2021**, *264*, 114938. [CrossRef]
71. Housecroft, C.E.; Sharpe, A.G. *Química Inorgânica*, 4th ed.; LTC, 2013; Volume 1, p. 6. Available online: https://www.ifsc.edu.br/documents/35977/1670122/PPC+do+CST+em+Processos+Qu%C3%ADmicos/db5f1bdb-c035-471f-aa4f-8c8557f9a917 (accessed on 1 February 2022).
72. Stöwe, K.; Weber, M. Niobium, tantalum, and tungsten doped tin dioxides as potentialn support materials for fuel cell cata-lyst applications. *Z. Anorg. Allg. Chem.* **2020**, *646*, 1470–1480. [CrossRef]
73. Bolzan, A.A.; Fong, C.; Kennedy, B.; Howard, J.C. Structural Studies of Rutile-Type Metal Dioxides. *Acta Crystallogr. B* **1995**, *53*, 373–380. [CrossRef]
74. Yang, C.; Fan, Y.; Li, P.; Gu, Q.; Li, X. Freestanding 3-dimensional macro-porous SnO_2 electrodes for efficient electrochemical degradation of antibiotics in wastewater. *Chem. Eng. J.* **2021**, *422*, 130032. [CrossRef]
75. Liu, B.; Li, K.; Luo, Y.; Gao, L.; Duan, G. Sulfur spillover driven by charge transfer between AuPd alloys and SnO_2 allows high selectivity for dimethyl disulfide gas sensing. *Chem. Eng. J.* **2021**, *420*, 129881. [CrossRef]
76. Qiua, H.; Zhenga, H.; Jin, Y.; Yuana, Q.; Zhanga, X.; Zhao, C.; Wangb, H.; Jia, M. Mesoporous cubic SnO_2-CoO nanoparticles deposited on graphene as anode materials for sodium ion batteries. *J. Alloys Compd.* **2021**, *874*, 159967. [CrossRef]
77. Kim, M.J.; Kim, T.G. Fabrication of Metal-Deposited Indium Tin Oxides: Its Applications to 385 nm Light-Emitting Diodes. *Appl. Mater. Interfaces* **2016**, *8*, 5453–5457. [CrossRef]
78. Haq, S.; Rehman, W.; Waseem, M.; Shah, A.; Khan, A.R.; Rehman, M.; Ahmad, P.; Khan, B.; Ali, G. Green synthesis and characterization of tin dioxide nanoparticles for photocatalytic and antimicrobial studies. *Mater. Res. Express* **2020**, *7*, 025012. [CrossRef]
79. Hojamberdiev, M.; Czech, B.; Goktas, A.C.; Yubuta, K.; Kadirova, Z.C. SnO_2@ZnS photocatalyst with enhanced photocatalytic activity for the degradation of selected pharmaceuticals and personal care products in model wastewater. *J. Alloys Compd.* **2020**, *827*, 154339. [CrossRef]
80. Bezzerrouk, M.A.; Bousmaha, M.; Akriche, A.; Kharroubi, B.; M'hamed, G. Hybrid structure comprised of SnO_2, ZnO and Cu_2S thin film semiconductors with controlled optoelectric and photocatalytic properties. *Thin Solid Films* **2013**, *542*, 31–37.
81. Han, K.; Peng, X.-L.; Li, F.; Yao, M.-M. SnO_2 Composite Films for Enhanced Photocatalytic Activities. *Catalysts* **2018**, *8*, 453. [CrossRef]
82. Haya, S.; Brahmia, O.; Halimi, O.; Sebais, M.; Boudine, B. Sol–gel synthesis of Sr-doped SnO_2 thin films and their photocatalytic properties. *Mater. Res. Express* **2017**, *4*, 106406. [CrossRef]
83. Raj, I.L.P.; Revathy, M.S.; Christy, A.J.; Chidhambaram, N.; Ganesh, V.; AlFaify, S. Study on the synergistic effect of terbium-doped SnO_2 thin film photocatalysts for dye degradation. *J. Nanopart. Res.* **2020**, *22*, 359. [CrossRef]
84. Va-divel, S.; Rajarajan, G. Effect of Mg doping on structural, optical and photocatalytic activity of SnO_2 nanostructure thin films. *J. Mater. Sci. Mater. Electron.* **2015**, *26*, 3155–3162. [CrossRef]
85. Li, Q.; Zhao, H.; Sun, H.; Zhao, X.; Fan, W. Doubling the photocatalytic performance of SnO_2 by carbon coating mixed-phase particles. *RSC Adv.* **2018**, *8*, 30366–30373. [CrossRef]
86. Hermawan, A.; Asakura, Y.; Inada, M.; Yin, S. One-step synthesis of micro-/mesoporous SnO_2 spheres by solvothermal method for toluene gas sensor. *Ceram. Int.* **2019**, *45*, 15435–15444. [CrossRef]
87. Hermawan, A.; Asakura, Y.; Inada, M.; Yin, S. A facile method for preparation of uniformly decorated-spherical SnO_2 by CuO nanoparticles for highly responsive toluene detection at high temperature. *J. Mater. Sci. Technol.* **2020**, *51*, 119–129. [CrossRef]
88. Wang, X.; Fan, H.; Ren, P.; Li, M. Homogeneous SnO_2 core–shell microspheres: Microwave-assisted hydrothermal synthesis, morphology control and photocatalytic properties. *Mater. Res. Bull.* **2014**, *50*, 191–196. [CrossRef]
89. Rodrigues, E.C.P.E.; Olivi, P. Preparation and characterization of Sb-doped SnO_2 films with controlled stoichiometry from polymeric precursors. *J. Phys. Chem. Solids* **2003**, *64*, 1105–1112. [CrossRef]
90. Akram, M.; Saleh, A.T.; Ibrahim, W.A.W.; Awan, A.S.; Hussain, R. Continuous microwave flow synthesis (CMFS) of nano-sized tin oxide: Effect of precursor concentration. *Ceram. Int.* **2016**, *42*, 8613–8619. [CrossRef]
91. Fatimah, I.; Purwiandono, G.; Jauhari, H.M.; Aisyah, A.A.; Sagadevan, P.; Oh, W.-C.; Doong, R.-A. Synthesis and control of the morphology of SnO_2 nanoparticles via various concentrations of Tinospora cordifolia stem extract and reduction method. *Arab. J. Chem.* **2022**, *15*, 103738. [CrossRef]

92. Abdelkader, E.; Nadjia, L.; Naceur, B.; Noureddine, B. SnO_2 foam grain-shaped nanoparticles: Synthesis, characterization and UVA light induced photocatalysis. *J. Alloys Compd.* **2016**, *679*, 408–419. [CrossRef]
93. Najjar, M.; Hosseini, H.A.; Masoudi, A.; Sabouri, Z.; Mostafapour, A.; Khatami, M.; Darroudi, M. Green chemical approach for the synthesis of SnO_2 nanoparticles and its application in photocatalytic degradation of Eriochrome Black T dye. *Optik* **2021**, *242*, 167152. [CrossRef]
94. Kumar, M.; Mehta, A.; Mishra, A.; Singh, J.; Rawat, M.; Basu, S. Biosynthesis of tin oxide nanoparticles using Psidium Guajava leave extract for photocatalytic dye degradation under sunlight. *Mater. Lett.* **2018**, *215*, 121–124. [CrossRef]
95. Mahmood, H.; Khan, M.A.; Mohuddin, B.; Iqbal, T. Solution-phase growth of tin oxide (SnO_2) nanostructures: Structural, optical and photocatalytic properties. *Mater. Sci. Eng. B* **2020**, *258*, 114568. [CrossRef]
96. Wang, J.; Fan, H.-Q.; Yu, H.-W. Synthesis of Hierarchical SnO_2 Microflowers Assembled by Nanosheets and Their Enhanced Photocatalytic Properties. *Mater. Trans.* **2015**, *56*, 1911–1914. [CrossRef]
97. Costantino, F.; Armirotti, A.; Carzino, R.; Gavioli, L.; Athanassiou, A.; Fragouli, D. In situ formation of SnO_2 nanoparticles on cellulose acetate fibrous membranes for the photocatalytic degradation of organic dyes. *J. Photochem. Photobiol. A Chem.* **2020**, *398*, 112599. [CrossRef]
98. Mala, N.; Ravichandran, K.; Pandiarajan, S.; Srinivasan, N.; Ravikumar, B.; Nithiyadevi, K. Enhanced antibacterial and photocatalytic activity of (Mg+Co) doped tin oxide nanopowders synthesised using wet chemical route. *Mater. Technol.* **2017**, *32*, 1328082. [CrossRef]
99. Chu, L.; Fangfang Duo, F.; Zhang, M.; Wu, Z.; Sun, Y.; Wang, C.; Donga, S.; Sun, J. Doping induced enhanced photocatalytic performance of SnO_2:Bi^{3+}quantum dots toward organic pollutants. *Colloids Surf. A* **2020**, *589*, 124416. [CrossRef]
100. Ragupathy, S.; Manikandan, V.; Devanesan, S.; Ahmed, M.; Ramamoorthy, M.; Priyadharsan, A. Enhanced sun light driven photocatalytic activity of Co doped SnO_2 loaded corn cob activated carbon for methylene blue dye degradation. *Chemosphere* **2022**, *295*, 133848. [CrossRef]
101. Ragupathy, S.; Sathya, T. Photocatalytic decolorization of brilliant green by Ni doped SnO_2 nanoparticles. *J. Mater. Sci. Mater. Electron.* **2018**, *29*, 8710–8719. [CrossRef]
102. Soltan, W.B.; Ammar, S.; Olivie, C.; Toupance, T.; Soltan, W.B. Influence of zinc doping on the photocatalytic activity of nanocrystalline SnO_2 particles synthesized by the polyol method for enhanced degradation of organic dyes. *J. Alloys Compd.* **2017**, *729*, 638–647. [CrossRef]
103. Baig, A.; Ali Baig, A.; Rathinam, V.; Palaninathan, J. Fabrication of Zr-doped SnO_2 nanoparticles with synergistic influence for improved visible-light photocatalytic action and antibacterial performance. *Appl. Water Sci.* **2020**, *10*, 54. [CrossRef]
104. Borker, P.; Salker, A.; Gaokar, R.D. Sunlight driven improved photocatalytic activity of Mn doped SnO_2 nanowires. *Mater. Chem. Phys.* **2021**, *270*, 124797. [CrossRef]
105. Abdel-Messih, M.F.; Ahmed, M.A.; El-Sayed, A.S. Photocatalytic decolorization of Rhodamine B dye using novel mesoporous SnO_2–TiO_2 nano mixed oxides prepared by sol–gel method. *J. Photochem. Photobiol. A Chem.* **2013**, *260*, 1–8. [CrossRef]
106. Subashri, K.; Santhi, N. Synthesis and characterization of CrO_4-SnO_2 nanocomposites and their industrial and electrochemical applications. *Mater. Today Proc.* **2022**, *48*, 443–453. [CrossRef]
107. Wang, X.; He, Y.; Xu, L.; Xia, Y.; Gang, R. SnO_2 particles as efficient photocatalysts for organic dye degradation grown in-situ on g-C_3N_4 nanosheets by microwave-assisted hydrothermal method. *Mater. Sci. Semicond. Process.* **2021**, *121*, 105298. [CrossRef]
108. Onwudiwe, D.C.; Oyewo, O.A. Facile synthesis and structural characterization of zinc stannate/tin oxide and zinc stannate/tin composites for the removal of methylene blue from water. *Mater. Res. Express* **2019**, *6*, 125025. [CrossRef]
109. Akti, F. Photocatalytic degradation of remazol yellow using polyaniline–doped tin oxide hybrid photocatalysts with diatomite support. *Appl. Surf. Sci.* **2018**, *455*, 931–939. [CrossRef]
110. Palai, A.; Panda, N.R.; Sahu, D. Novel ZnO blended SnO_2 nanocatalysts exhibiting superior degradation of hazardous pollutants and enhanced visible photoemission properties. *J. Mol. Struct.* **2021**, *1244*, 131245. [CrossRef]
111. Lahmar, H.; Benamira, M.; Douafer, S.; Akika, F.Z.; Hamdi, M.; Avramova, I.; Trari, M. Photocatalytic degradation of Crystal Violet dye on the novel $CuCr_2O_4$/SnO_2 hetero-system under sunlight. *Optik* **2020**, *219*, 165042. [CrossRef]
112. Steplinpaulselvin, S.; Rajaram, R.; Silambarasan, T.S.; Chen, Y. Survival assessment of simple food webs for dye wastewater after photocatalytic degradation using SnO_2/GO nanocomposites under sunlight irradiation. *Sci. Total Environ.* **2020**, *721*, 137805.
113. Li, Z.; Zhao, Y.; Hua, L.; Bi, D.; Xie, J.; Zhou, Y. Hollow SnO_2/Zn_2SnO_4 cubes with porous shells towards n-butylamine sensing and photocatalytic applications. *Vacuum* **2020**, *182*, 109693. [CrossRef]
114. Rani, A.; Singh, K.; Patel, A.S.; Chakraborti, A.; Kumar, S.; Ghosh, K.; Sharma, P. Visible light driven photocatalysis of organic dyes using SnO_2 decorated MoS_2 nanocomposites. *Chem. Phys. Lett.* **2020**, *738*, 136874. [CrossRef]
115. Manjunatha, A.S.; Pavithra, N.S.; Shivanna, M.; Nagaraju, G.; Ravikumar, C.R. Synthesis of Citrus Limon mediated SnO_2-WO_3 nanocomposite: Applications to photocatalytic activity and electrochemical sensor. *J. Environ. Chem. Eng.* **2020**, *8*, 104500. [CrossRef]